Aus der Klinik für Nephrologie

der Medizinischen Fakultät Charité – Universitätsmedizin Berlin

DISSERTATION

Ex vivo measurement of biomechanical properties during vascular calcification

Ex vivo Messung biomechanischer Eigenschaften bei Gefäßverkalkung

zur Erlangung des akademischen Grades

Doctor medicinae (Dr. rer. medic.)

vorgelegt der Medizinischen Fakultät

Charité – Universitätsmedizin Berlin

von

Jinwen Zhou

aus Hanzhong, Shaanxi, China

Datum der Promotion: 25.06.2023

Content

List of tables

List of figures

List of abbreviations

Abbreviation	Meaning
AAC	Abdominal aortic calcium
ALP	Alkaline phosphatase
AUC	Area under curve
AZA	Azathioprine
BMP2	Bone morphogenetic protein 2
CAC	Coronary artery calcium
CaCl2	Calcium chloride
CaCS	Coronary artery calcification score
CAM	Calcification medium
Cbfa1	Core-binding factor subunit alpha-1
CKD	Chronic kidney disease
Col1	Type 1 collagen
COM	Control medium
CRD	Chronic renal disease
CRIC	Chronic Renal Insufficiency Cohort
CVD	Cardiovascular disease
DCCT/EDIC	Diabetes Control and Complications Trial/Epidemiology of Diabetes Interventions and Complications
DMA	Dynamic mechanical analysis
ECM	Extracellular matrix
ENPP1	Ectonucleotide pyrophosphatase/phosphodiesterase 1
ESRD	End-stage renal disease
FGF23	Fibroblast growth factor 23
IMPROVE-CKD	Impact of Phosphate Reduction On Vascular End-points in CKD
KDIGO	The kidney disease improving global outcomes
LVH	Left ventricular hypertrophy

MAGP	Microfibril-associated glycoprotein
MMP	Matrix metalloproteinases
MMS	Monckeberg medial sclerosis
6-MP	6-mercaptopurine
MSCT	Multislice spiral computed tomography
NLRP3	NLR family pyrin domain containing 3
OCC	Osteo-chondrogenic cell
OCN	Osteocalcin
OPG	Osteoprotegerin
OPN	Osteopontin
PBS	Phosphate-buffered saline
PiT-1	Pituitary-specific positive transcription factor 1
PPi	Pyrophosphate
ROS	Reactive oxygen specifies
Runx2	Runt-related transcription factor 2
SASP	Senescence-associated secretory phenotype
SM22α	Smooth Muscle 22α
SMC	Smooth muscle cell
Sox9	Sex determining region Y-box 9
SVM	Small vessel myograph
α-SMA	α-Smooth muscle actin
TNAP	Tissue nonspecific alkaline phosphatase
TNFα	Tumor necrosis factor α
VC	Vascular calcification
VCi	Vascular calcification intima
VCm	Vascular calcification media
VSMC	Vascular smooth muscle cell
VSMC-MV	Vascular smooth muscle cell-derived matrix vesicle
WHO	World Health Organization

Zusammenfassung

Hintergrund: Gefäßverkalkung (VC) ist die abnormale Ablagerung von Kalziumphosphatsalzen in den Blutgefäßen, die zu einer hohen kardiovaskulären Sterblichkeits- und Morbiditätsrate bei Patienten mit chronischer Nierenerkrankung beiträgt. Bislang fehlen wirksame Behandlungsmöglichkeiten der VC in der klinischen Routine. Die Untersuchung der VC-Pathogenese ist daher von zentraler Bedeutung. Die komplexe Struktur und Zusammensetzung der Gefäßwand bietet einzigartige biomechanische Eigenschaften. Die physiologische Struktur der Blutgefäße ist die Voraussetzung für die Aufrechterhaltung der biomechanischen Eigenschaften. VC kann die normale Struktur von Blutgefäßen schädigen, was zu Veränderungen der biomechanischen Eigenschaften führt. Dies ist hauptsächlich auf den Einfluss von VC auf elastische Fasern und Kollagenfasern zurückzuführen. Derzeit sind jedoch nur wenige Methoden verfügbar, die die Veränderungen der biomechanischen Eigenschaften der Arterienwand während der VC beschreiben. Diese Studie zielt darauf ab, diese Lücke zu schließen und eine Methode zur Messung der Veränderungen der biomechanischen Eigenschaften der Arterienwand während der Gefäßverkalkung zu validieren.

Methode: Zur Messung der biomechanischen Eigenschaften der Arterienwand erfolgt die Überwachung durch den Small-Vessel-Myograph. Fünf biomechanische Parameter (E_{low}, E_{high}, AUC, $\sigma_{breaking\ point}$, $\lambda_{breaking\ point}$) in der Spannungs-Dehnungs-Kurve wurden berechnet. Die Stimulation der thorakalen Rattenaorta erfolgte in Zeit-Wirkungs-Kurven mittels verschiedener Induktoren. Sowohl die biomechanischen Eigenschaften, als auch der Kalziumgehalt, als akuteller „Goldstandard“ wurde gemessen, um die Methode zu validieren.

Ergebnisse: Unter basalen, nicht stimuierten, Bedingungen waren sowohl die biomechanischen Eigenschaften als auch der Kalziumgehalt in verschiedenen

Bereichen der Aorta nicht signifikant verschieden. Nach Stimulation der Aortenringe mit CAM (Calcification medium) für 14 Tage, konnte eine Kalzifizierung und Veränderung der biomechanischen Eigenschaften induzierte werden, die sich in den einzelen Bereichen der thorakalen Aorta nicht signifikant unterschied.

Eine Zeit-Wirkungs-Kurve für die Stimulation mit CAM und COM (Kontroll medium) zeigte eine zeitabhängige Induktion der Kalzifizierung über 3, 7, 14 und 21 Tage. Der hohe Phosphatgehalt im CAM verändert die biomechanischen Eigenschaften der Gefäßwand zeitabhängig, die mit einem hohen Kalziumgehalt in der Arterienwand einhergehen.

Für einen aus Voruntersuchungen bereits bekannten weiteren Induktor der VC, Azathioprin, konnte ebenfalls eine Veränderung der biomechanischen Eigenschaften der Arterienwand im Kalzifizierungsprozess bestätigt werden.

Schlussfolgerung: Diese Studie erstellte und validierte ein Protokoll zur Erkennung von Veränderungen der biomechanischen Eigenschaften der Gefäßwand während der VC. Dieses Protokoll erweitert die aktuellen Analysewerkzeuge im Forschungsfeld der VC und kann die Veränderungen der biomechanischen Eigenschaften während der VC anhand physiologischer Gefäßeigentschaften beschreiben.

Abstract

Background: Vascular Calcification (VC) is the abnormal deposition of calcium -phosphate salts in the blood vessel, contributing to high cardiovascular mortality and morbidity rates among patients with chronic kidney disease (CKD). As effective treatment options are currently lacking, an understanding of VC pathogenesis plays a key role. The complicated composition and structure of the vascular wall provide special biomechanical properties. The physiological structure of blood vessels is the prerequisite for maintaining biomechanical properties. VC can damage the normal structure of blood vessels, leading to changes in biomechanical properties. This is largely due to the influence of VC on elastic fibers and collagen fibers. However, currently few methods that describe the changes in biomechanical properties of the arterial wall during VC are available. This study aims to bridge that gap and validate a method to measure the changes in biomechanical properties of the arterial wall during VC.

Method: To measure the biomechanical properties of the arterial wall, monitoring is done through the small-vessel-myograph. Five biomechanical parameters (E_{low}, E_{high}, AUC, $\sigma_{breaking\ point}$, $\lambda_{breaking\ point}$) in the stress-stretch curve were calculated. The thoracic rat aorta was stimulated in time-response curves using various inducers. Both the biomechanical properties and the calcium content were measured in order to validate the method.

Results: Firstly, under basal (non-stimulated conditions), both the biomechanical properties and the calcium content in different areas of the aorta were not significantly different. After stimulation of the aortic rings with CAM (Calcification medium) for 14 days, calcification and changes in biomechanical properties could be induced, which did not differ significantly in the individual areas of the thoracic aorta. Then, we compared the biomechanical properties and calcium content between CAM and COM (Control medium) at 3, 7, 14, and 21 days, respectively. High phosphate can affect biomechanical properties

during VC, which is related to incubation time. Finally, we use another VC inducer (Azathioprine), which can also affect biomechanical properties during VC and is related to incubation time. However, this effect requires the presence of high phosphate.

Conclusion: This study established and validated a protocol for the detection of changes in biomechanical properties of the vessel wall during VC. This protocol expands the current analytical tools in the research field of VC, and can directly describe the changes in biomechanical properties during VC.

1. Introduction

According to the World Health Organization (WHO), cardiovascular disease (CVD) is the leading cause of noncommunicable diseases, killing approximately 17.9 million people each year [1]. As compared with the general population, the morbidity and mortality rates of CVD are higher among patients with chronic kidney disease (CKD). The higher morbidity and mortality rates of CVD in CKD patients are primarily due to extensive pathological deposition of calcium phosphate resulting in vascular calcification (VC) [2].

1.1. Definitions and clinical impact of vascular calcification

VC occurs in the tunica media layer (arteriosclerosis) and tunica intima layer (atherosclerosis) depending on the location of the calcium phosphate deposition [3]. Vascular calcification intima (VCi), called atherosclerosis, is commonly caused by lipid accumulation, in which punctate occurs and is located in the walls of the coronary artery, carotid artery, and other large-sized arteries. Atherosclerosis is related to the proliferation and migration of T cells, macrophages, smooth muscle cells (SMC), and endothelial dysfunction. Initial microcalcification is most likely initiated by smooth muscle cell apoptosis, and then macrophage apoptosis within the necrotic core of the plaque, which leads to larger punctuate calcification [4]. Vascular calcification media (VCm), called monckeberg medial sclerosis (MMS) or arteriosclerosis, is characterized by the linear distribution of hydroxyapatite [$Ca_{10}(PO_4)_6OH_2$] and magnesium-containing whitlockite [$(Ca, Mg)_3(PO_4)_2$] along with the elastic layer. It often appears in the walls of the femoral artery, ovarian artery, parathyroid artery, and other medium- to small-sized arteries [5]. Arteriosclerosis is related to the proliferation, migration, and osteogenesis of vascular smooth muscle cells (VSMC), in which immune cells seem to play a minor role [6, 7]. Different kinds of VC are also associated with different clinical consequences. VCm is associated with increasing vessel stiffness, wide pulse pressure, and left ventricular hypertrophy (LVH), whereas VCi is associated with ischemic heart

disease, infarction, and revascularization [8]. (Figure 1 schematically summarizes the intimal and medial calcification progression.)

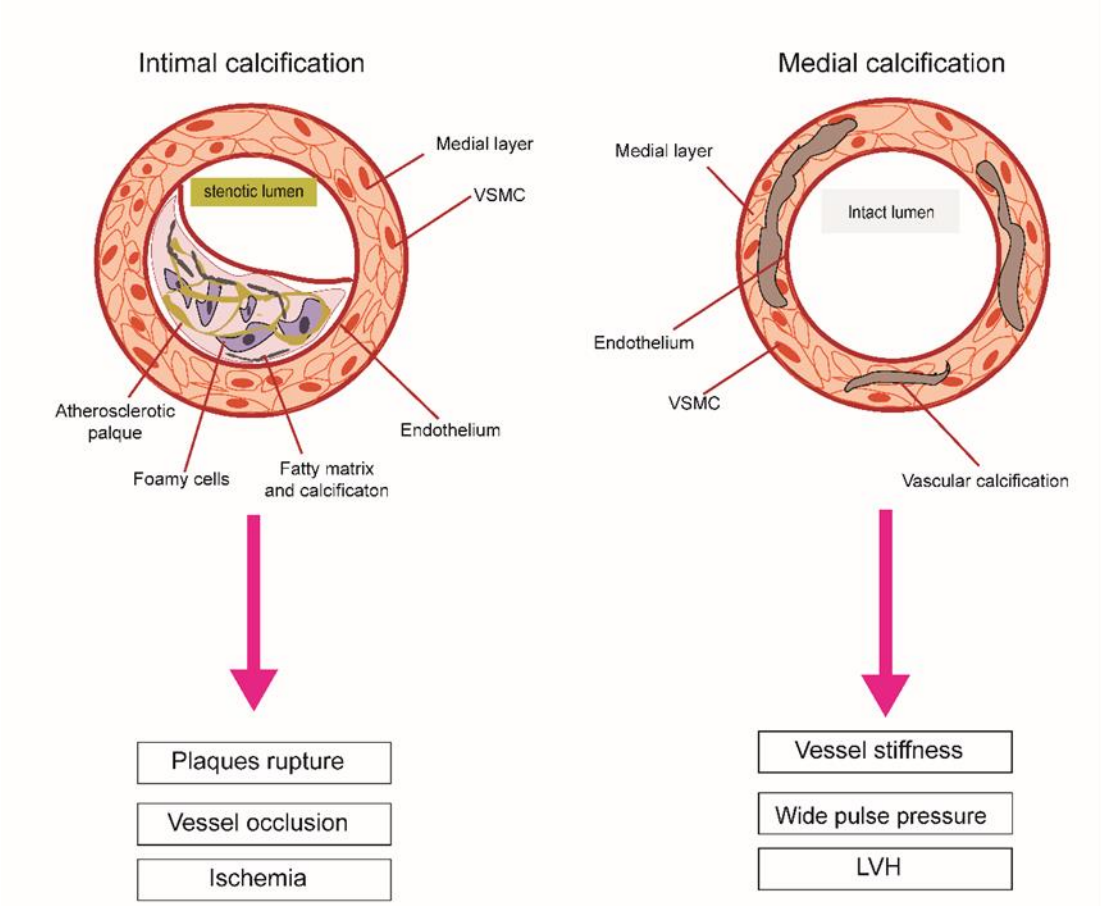

Figure 1. Schematic representation of intimal and medial calcification. (Modified from Cozzolino M, et al., The Key Role of Phosphate on Vascular Calcification. Toxins. 2019; 11(4):213 [9].)

As a highly prevalent vascular pathophenotype, VC is regarded as part of the manifestation of the ageing process and increases mortality in older people, atherosclerotic heart disease, diabetes mellitus, and CKD [10]. In a long follow-up study, abdominal aortic calcium (AAC) was identified in 1049 men and 1466 women (mean age, 61 years) by multidetector computed tomography, which is considered an independent predictor of cardiovascular morbidity and mortality [11]. 15-year-long follow-up research involving a cohort of 9,715 adults described the effectiveness of coronary artery calcium (CAC) scores in predicting long-term mortality in people with no symptoms of coronary artery disease. The all-cause mortality was 3% among persons without coronary

artery calcification, whereas 28% among persons suffering from high levels of coronary artery calcification [12]. The CAC scores >100 Agatston units were significantly associated with a higher risk of CVD events in Diabetes Control and Complications Trial/Epidemiology of Diabetes Interventions and Complications (DCCT/EDIC) participants [13].

Clinical evidence has also demonstrated that VC is an independent predictor of cardiovascular morbidity and mortality in patients with CKD or end-stage renal disease (ESRD). In the Impact of Phosphate Reduction On Vascular End-points in CKD (IMPROVE-CKD) study, a high risk of cardiovascular events was found to be associated with high values of carotid-femoral pulse-wave velocity and abdominal aortic calcification (AAC) [14]. Coronary calcifications (calcium score > 100 U) in patients with CKD who are not undergoing dialysis have a higher rate of cardiac events than patients with less calcified patients (calcium score < 100 U) [15]. The prospective study including 110 stable ESRD patients on hemodialysis indicated that the presence and extent of VC in different regions were strong predictors of cardiovascular and all-cause mortality [16]. In children and young adults with ESRD, higher coronary-artery calcification is related to higher CVD events [17]. However, there are currently no available therapies that can regress the process of VC. It is very important for us to understand the process of VC, which may lead to the development of novel therapies to prevent or regress VC.

1.2. Changes in biomechanical properties of the vessel during vascular calcification

As we know, arteries consist of three distinct layers from inside to outside, including the tunica intima, the tunica media, and the tunica adventitia. The proportion of the structural components and the thickness of the wall is different in small-, medium-, and large-sized arteries, but in general, the innermost layer is composed of endothelial cells covering the luminal surfaces of blood vessels. The tunica media consists of circumferentially arranged elastin and collagen

fibers, as well as smooth muscle cells (SMC).The outer layer is composed of fibroblasts, elastin, and collagen fibers that are organized longitudinally in the form of wavy bundles [18, 19]. Propagated blood flow and pulling of surrounding tissue can build mechanical tension in blood vessels [20-22]. Conventional mechanical tests for vessels include, but are not limited to, tensile, tensile stress-relaxation, compression, burst pressure, dynamic compliance, dynamic mechanical analysis (DMA), and creep. The main difference lies in the nature of the applied loading or deformation, whether it is compressive or tensile; constant or incremental, and cyclic; uniaxial or pressure-based.

The complicated composition and structure of the vascular wall provide a special mechanical response, any disturbance can significantly compromise its mechanical response. The normal structure of blood vessels is a prerequisite for maintaining a normal mechanical response. The passive mechanical response (resilience and tensile strength of vessels) is conferred on the arterial extracellular matrix (ECM), which is composed mainly of elastic fibers and collagen fibers. VC can damage the normal structure of blood vessels, leading to dysfunction of passive mechanical response and changes in biomechanical properties. This is largely due to the influence of VC on elastic fibers and collagen fibers [23]. During VC, elastic fibers are able to calcify and injure due to the presence of mineralization nucleation sites including sulfhydryl and carboxyl groups, matrix glycoproteins, glycosaminoglycans, lipoproteins, calcium-binding proteins, and matrix Gla protein [24-31]. Collagens are a family of 28 kinds of collagens named using the Roman numerals I~XXVIII, which are the most abundant proteins produced by mesenchymal and epithelial cells in the body [32, 33]. High expression of collagen type I accelerates VC, whereas collagen type IV and type XIV inhibit mineral deposition [34-36]. The collagen I expression is higher under high levels of phosphate, calcium, and uric acid [34-36]. These effects are linked with the calcium/phosphate-induced osteochondrocytic transdifferentiation of VSMC and change some makers,

including recombinant protein of human runt-related transcription factor 2 (Runx2), recombinant protein of human SRY (sex determining region Y)-box 9 (Sox9), α-smooth muscle actin (α-SMA), and smooth muscle 22α (SM22α) expression [37]. When VSMC were cultured in purified collagen I medium, the formation of mineralization nodules representing the occurrence of VC and the tissue nonspecific alkaline phosphatase (TNAP) representing VSMC phenotypic alterations increased [38]. However, current research focused on studying the changes in the expression of collagen or elastin fibers in vitro, there is limited research on the changes in biomechanical properties based on collagen or elastin fibers during VC ex vivo.

1.3. The effect of phosphate on vascular calcification

VC is a complex process of the pathological accumulation of calcium-phosphate complexes in the vasculature, which was previously thought to be a passive degenerative process, however, recent studies illustrate an active biomineralization process, similar to osteogenesis [39]. VC progression in CKD is considered to be a disruption of mineral homeostasis, especially high phosphate load. Phosphorus appears to be involved in several mechanisms including promoting and triggering VSMC from the contractile phenotype to the osteochondrogenic phenotype, promoting VSMC extracellular matrix mineralization, inducing VSMC apoptosis, losing circulating inhibitors of calcification, and regulating hormones. Several studies in vitro using VSMC have demonstrated phosphorus-induced activation of pro-calcific intracellular signaling pathways that directly affect VC [40, 41]. High phosphate enhances the osteogenic transition of VSMC by upregulating the type III sodium-dependent phosphate transporter to raise intracellular levels of inorganic phosphate (Pi), decrease SM22α expression, and increase Runx2 expression [42]. The production of matrix metalloproteinases and cysteine proteases induced by high phosphorus leads to the degradation of matrix proteins, the production of biologically active elastin peptides, and the synthesis of collagen,

resulting in a collagen-rich extracellular matrix [43, 44]. Under high-phosphate circumstances, the VSMC may generate apoptotic bodies, which could serve as a nidus for calcium phosphate precipitation. Phosphate also regulates different intracellular signaling resulting in apoptosis, while inhibiting apoptosis inhibits calcification [45-49]. In vivo studies showed that phosphate disbalance promotes VC in uremic rodents. Serum phosphate levels can be maintained in the physiological range by hormonal regulation, including but not limited to vitamin D, fibroblast growth factor 23 (FGF23), and α-Klotho. Recent studies on genetically modified mouse models that physiologically decrease or increase serum phosphate concentration through hormones that affect physiological phosphate metabolism provide more evidence for the involvement of phosphate in the VC process [50].

A large body of clinical evidence also supports the idea that phosphate plays a central role in VC, particularly in patients with CKD. Adeney K.L. et al. investigated 439 participants in the Multi-Ethnic Study of Atherosclerosis who had moderate CKD but no clinical cardiovascular disease. The higher serum phosphate concentration, although in the normal range, is independently and strongly associated with the higher prevalence of coronary artery, thoracic, aortic, and mitral valve calcification [51]. Among 1123 CKD patients in the Chronic Renal Insufficiency Cohort (CRIC) study, coronary artery calcification (CAC) is associated with reduced kidney function, calcium and phosphate metabolism disorders, and inflammation [52]. In the prospective study on hemodialysis patients, hyperphosphatemia results in the synthesis and secretion of tumor necrosis factor α (TNFα) by monocytes via regulating the pituitary-specific positive transcription factor 1 (PiT-1) pathway to elevated systemic inflammatory levels, which may further aggravate VC. In patients with peritoneal dialysis, the coronary artery calcification score (CaCS) measured by multislice spiral computed tomography (MSCT) is associated with hyperphosphatemia [53]. It is possible to lower the serum phosphate level to

the normal range by restricting dietary phosphate intake, reducing its intestinal absorption, and removing it by dialysis to regress VC according to kidney disease improving global outcomes (KDIGO) guidelines [54]. In summary, studying the pathogenesis of high phosphate-induced VC might help find potential therapies for the disease.

1.4. The effect of Azathioprine on vascular calcification

Azathioprine (AZA), a pro-drug of 6-mercaptopurine, was synthesized in 1957 [55]. It is from the research of Nobel Prize laureates George Herbert Hitchings and Gertrude Elion in 1957. Initially, 6-mercaptopurine (6-MP) was studied as a chemotherapeutic drug for leukemia treatment, and then Robert Schwartz discovered that the antibodies of rabbits treated with 6-mercaptopurine tended to decrease [56]. In further investigation, 6-mercaptopurine was found to reduce the risk of transplant rejection. Azathioprine is currently used as an immunosuppressive drug in the treatment of rejection after renal transplantation. After successful renal transplantation, the risk of CVD is lower as compared to patients with ERSD, but the risk is still higher in comparison to an age-matched population with normal kidney function. The possible reason is that the immunosuppressive drug exacerbates cardiac risk [57]. A recent longitudinal study that assessed the evolution of coronary artery and thoracic aorta calcification and their determinants in kidney transplant patients has shown that VC progression is substantial within 4 years after kidney transplant [58]. In our previous studies, we have already demonstrated that AZA and its metabolites induce the production of reactive oxygen species, intracellular activation of mitogen-activated kinases, and phosphorylation of the core-binding factor subunit alpha-1 (Cbfa1) resulting in vascular mineralization in vitro and ex vivo models [59]. Recently, we also demonstrated that the rat model treated with AZA for 24 weeks produced calcium deposition, and increased proinflammatory cytokines such as interleukin (IL)-1β and IL-6. These processes are dependent on the activity of the NLR family pyrin domain containing 3 **(**NLRP3)

inflammasome [60]. However, there is limited knowledge about the effect of AZA on biomechanical properties during VC. In this study, we investigated the influence of AZA on biomechanical properties during VC to provide further evidence for the effect of AZA treatment on the vascular structure.

1.5. Experimental analysis of vascular calcification

To better investigate the underlying mechanisms in the progression of VC, and evaluate compounds that might prevent or retard its onset or progression, many models have been established in the last few decades (as shown in Figure 2). Each of them has pros and cons [61]. Small rodents are often used as animal models for VC research in vivo. To reliably induce vascular calcification, it needs to come together in several models because small rodents have a high natural resistance to VC. The procedure is very complicated and causes extra pain for animals. Different cells involved in VC are often used as in vitro models. VC can be simply and effectively induced by stimulation in vitro and can also be easily and accurately arranged for each time or dose-concentration, providing insights into the molecular biological mechanisms involved in the process of VC. Nevertheless, the tissue around the cells is lost, and some processes involving cooperative interaction with the ECM and biomechanical properties cannot be investigated in vitro. The extracellular matrix provides the fundamental structure, mechanical load capacity, and physical support for cell adhesion and migration, and can influence phenotypic modulation and cell fate [74]. Although the lack of a comprehensive and precise understanding of the mechanisms responsible for the changes in biomechanical properties in the process of vascular calcification, ECM remodeling including elastin degradation and excessive collagen and glycosylation deposition is critical for the changes in biomechanical properties during VC.

Aortic rings from humans, bovines, mice, and rats are used to study VC ex vivo. Ex vivo experiments could build the bridge between traditional cell culture and animal models, which not only easily control the experimental conditions to

investigate pathways but also reduce the pain of animals in the experiment embodying the principle of the 3R rules [50]. The procedure is very simple and easy, taking less time to precisely evaluate vascular calcification, furthermore, maintaining the integrity of the vessel structure. The integrity of the vessel structure in the ex vivo experiment provides the possibility to study the change of biomechanical properties in the process of VC.

The goal of this work is to develop a method for investigating changes in biomechanical properties during the VC process in order to take full advantage of maintaining the vessel structure's integrity in the ex vivo experiment.

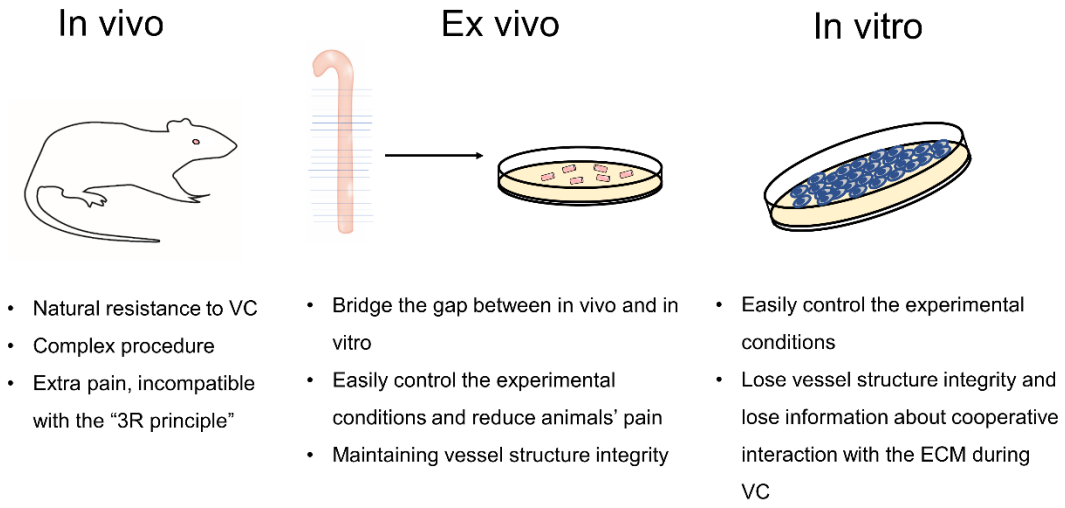

Figure 2. Schematically summarize of VC models

1.6. Introduction of small vessel myograph (SVM)

Until the mid-1970s, there were few methods to gain information about the mechanical, morphological, and pharmacological properties of small vessels. The information was only obtained from the large vessels. At that time only one of the mounting wires was used to measure the contraction force due to technological limitations in vitro. The investigation of small vessels was also precluded because relatively large wires (100-200 μm) could only be used. In addition, the mechanical trauma of the vessel may happen because of direct manipulation with dissecting instruments. Therefore, the studies of small vessels were limited to histological examination and in vivo perfusion

experiments.

In 1976, Professor M. J. Mulvany and Professor W. Halpern first described a new technique called the “wire myograph” that was used to study the function of mounted vessels ex vivo and made it possible to measure highly isometric vasomotor responses of vessels with internal diameters as small as 100 μm in different substances or procedures [62]. Subsequently, several improvements were applied to the myograph systems, wherein a more robust transducer, a new mechanical design, and a new electronic system were developed [62-65]. Now, the wire myograph has become a very useful and reliable technique to investigate vascular beds of endothelial function, vasoconstriction or vasodilation, and molecular pathways in a variety of animal species and diseases.

The Dual Wire Myograph System Model 620 (DMT 620) was used in this study. It is a four-channel myograph that allows the simultaneous study of four vessels in individual organ baths as shown in Figure 3. Around 2 mm rings were maintained in an organ bath and mounted by threading them over two parallel 40 μm tungsten wires between two jaws. One support is connected to a sensitive force transducer that records response force. The other support is connected to a micrometric screw that allows you to set up the stretch of the vessel. There are four acid-resistant stainless-steel chambers for separate independent testing, which ensures independence between the segments and experiments. Compounds can be added directly to the chamber without opening the cover to maintain a constant situation in the organ bath during the experiment.

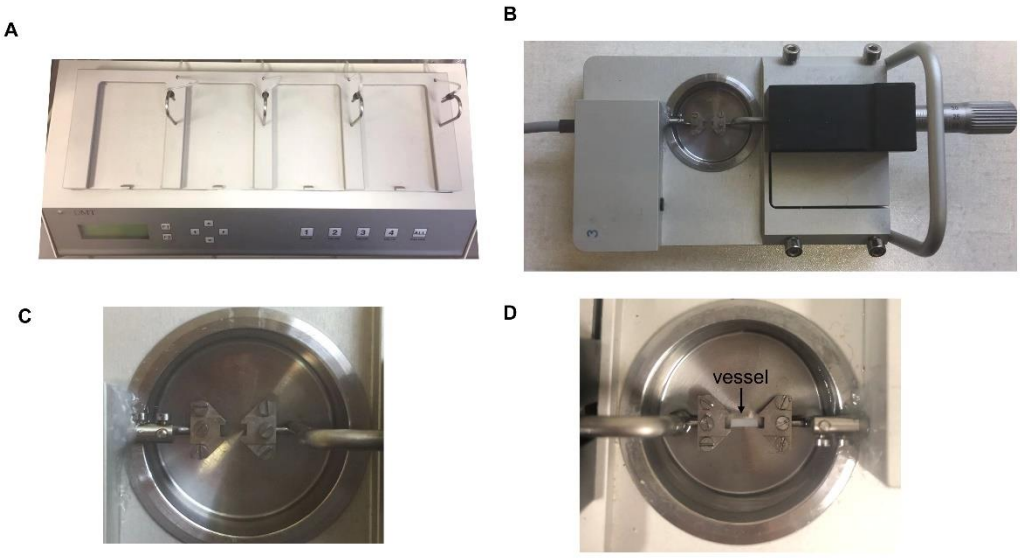

Figure 3. Structure of small vessel myograph.

1.7. Aim of the study

CKD patients have a higher prevalence of CVD. VC caused by the extensive pathological deposition of calcium-phosphate is one of the major reasons for the high morbidity and mortality rate of CVD in CKD patients. VC can damage the normal structure of blood vessels, leading to changes in biomechanical properties. Studying VC should take into account changes in biomechanical properties. However, there is a limited suitable method to investigate changes in biomechanical properties in the process of VC ex vivo experiment.

The study aims to:

1) Establish and validate a protocol for the detection of the changes in biomechanical properties of the vessel wall during VC using ex vivo setting.
2) Analysis of the changes in biomechanical properties of the vessel wall during VC with:
   a) High phosphate
   b) Azathioprine

2. Materials

Table 2-1. Materials and medium for ex vivo incubation

Medium and materials for ex vivo incubation	**Manufacturer**
Dulbecco's modified Eagle's medium (DMEM)	Biochrom AG, Berlin, Germany
Fetal calf serum (FCS)	Biochrom AG, Berlin, Germany
Penicillin/streptomycin	Biochrom AG, Berlin, Germany
NaH_2PO_4	Biochrom AG, Berlin, Germany
Ascorbic acid	Biochrom AG, Berlin, Germany
Azathioprine	Biochrom AG, Berlin, Germany

Table 2-2. Materials and medium for calcium content

Medium and materials for calcium content	**Manufacturer**
o-Cresolphthalein Complexone	Biochrom AG, Germany
HCl	Biochrom AG, Germany
NaOH	Biochrom AG, Germany
Phosphate-buffered saline	Biochrom AG, Germany
PBS	Biochrom AG, Germany

Table 2-3. Devices and software

Devices	**Manufacturer**	**Software**	**Manufacturer**
Small vessel myograph DMT 620	Danish Myo Technology, Aarhus, Denmark	GraphPad Prism statistical software v5.0	GraphPad, CA, USA
Analysis balance	Sartorius**,** Goettingen, Germany	Incubator	Heraeus, Germany
Microscope olympus CK 40	Olympus, Hamburg, Germany	Multiscan spectrum	Thermo Fisher Scientific, Germany

3. Methods

3.1. Animals preparation

The aortas were obtained from male Wistar rats with an average age of 1-3 months. The animals were kept in cages under standard conditions and fed with a normal chow diet with water ad libitum (temperature: 23±1°C, humidity: 45±10%). The protocol regarding the removal of organs from animals was approved by the local authorities (the Animal Committee of Charité Berlin, Berlin, Germany), which complied with "the guidelines of directive 2010/63/EU of the European Parliament on the protection of animals used for scientific purposes."

3.2. Aorta harvesting

To begin with, the animals were anesthetized with isoflurane (Forene®) by inhalation. Then, the animals were anesthetized with an intraperitoneal injection of Narcoren (400 mg/kg). The level of surgical anesthesia was checked using reflex tests as given by the modified Guedel scheme [66]. The thoracic and abdominal cavities were open. The lungs and heart were removed. The aorta was separated. The proximal end was brought as close to the heart as possible, and the distal end was separated above the diaphragm shown in Figure 4. The aorta was harvested by grasping soft tissue with forceps.

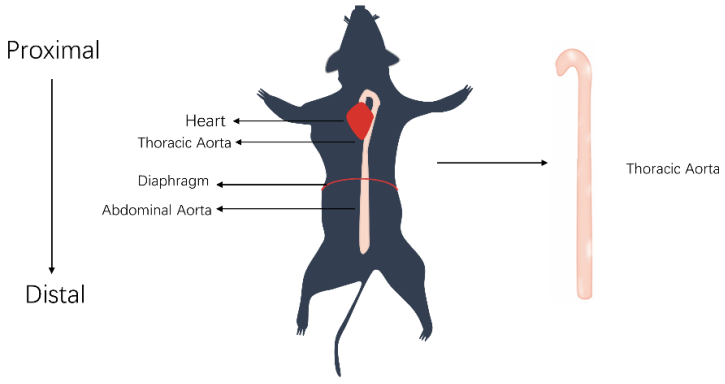

Figure 4. The schematic picture of thoracic aorta harvest. The proximal end was brought as close to the heart as possible, and the distal end was separated above the diaphragm.

3.3. Ex vivo incubation

The aorta was transferred to the cell culture dish with phosphate-buffered saline (PBS). The tissue surrounding the aorta was carefully removed with micro scissors and forceps without impairment under the stereomicroscope. To investigate whether the different areas in the thoracic aorta affect the biomechanical properties and calcium content. The thoracic aorta (removing the aortic arch) was cut into 18 rings of around 2 mm and numbered rings from the proximal to distal end before incubation, which were divided into different groups as shown in Figure 5. Before incubation (without stimulation), the biomechanical properties and calcium content of different areas in the thoracic aorta were compared. After 14 days of incubation with the calcification medium (CAM), the biomechanical properties and calcium content were also compared.

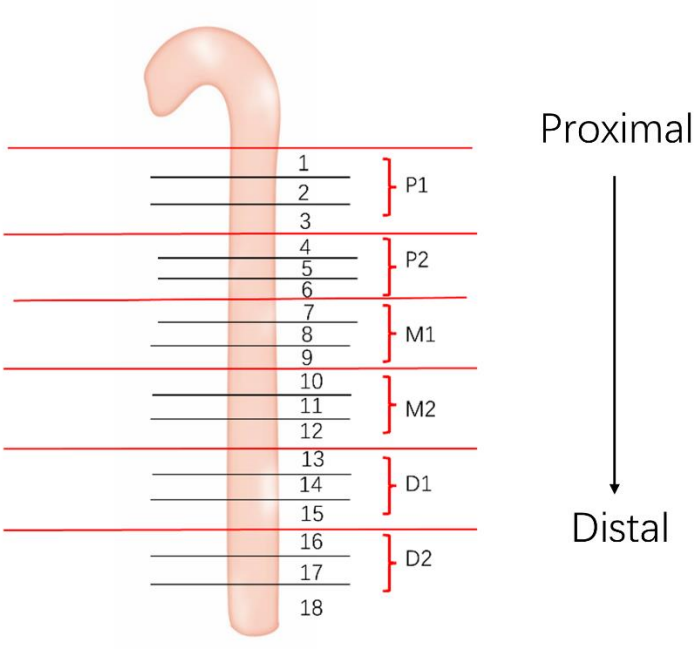

Figure 5. The schematic picture of different areas of the thoracic aorta. The thoracic aorta (removing the aortic arch) was cut into 18 rings to investigate whether different areas affect biomechanical properties and calcium content. The rings were numbered from proximal to the distal end and divided into P1, P2, M1, M2, D1, and D2.

To investigate how two vascular inducers (high-phosphate and AZA) affect biomechanical properties and calcium content. The thoracic aorta (removing

the aortic arch) was cut into 16 rings around 2 mm. The rings were divided into different groups with different mediums (CAM, CAM+AZA, COM, COM+AZA). The composition of the medium is shown in Table 3-1.

All buffers and media were added under sterile conditions. The rings were incubated at 37 °C, 5% carbon dioxide, and humidity conditions of 95% with different stimulations. The rings were harvested at different time points for 3, 7, 14, and 21 days.

Table 3-1. Composition of the incubation medium (CAM+AZA, CAM, COM, COM+AZA).

CAM+AZA	**CAM(Calcification medium)**	**COM (Control medium)**	**COM+AZA**
DMEM, 4.5 g/l Glucose	DMEM, 4.5 g/l Glucose	DMEM, 4.5 g/l Glucose	DMEM, 4.5 g/l Glucose
15% FCS	15% FCS	15% FCS	15% FCS
1% Pen/Strep	1% Pen/Strep	1% Pen/Strep	1% Pen/Strep
5 mM NaH_2PO_4	5 mM NaH_2PO_4	—	—
284 µM ascorbic acid	284 µM ascorbic acid	—	—
100 µM AZA	—	—	100 µM AZA

3.4. Passive mechanical response of the vessel

3.4.1. Preparation and mounting of the vessel

The procedure of preparation and mounting of vessels is shown in Figure 6.

1) The aorta was harvested from the rat and cut into 2 mm long rings.
2) One segment of stainless-steel wire 2.5 cm in length was prepared and put into the dish. Clamping the wire and carefully passing it through the ring lumen ensured that the wire remained straight and did not bend. The upper and lower sides of the wire were clamped by two forceps, and the ring was carefully transferred to the myograph chamber already filled with PBS solution.
3) The jaws were screwed apart to preserve the space for mounting. The ring was put in that space and moved closer to clamp the wire using the

micrometer. The wire at the corner of the unscrewed jaw was folded by the right-hand forceps and connected to the force transducer, and then the wire was wrapped clockwise around the screws of the right-side jaw and clamped by closing the screws.

4) Another wire was carefully passed through the lumen, and this step was repeated on the left side after adjusting the wire to make sure that they were at the same horizontal level. The vessel stays between two jaws. The two jaws couldn't touch each other.
5) The chamber was put into each channel and covered with its chamber cover. The heating and gas pump was turned on and the temperature probe was plugged into the chamber.

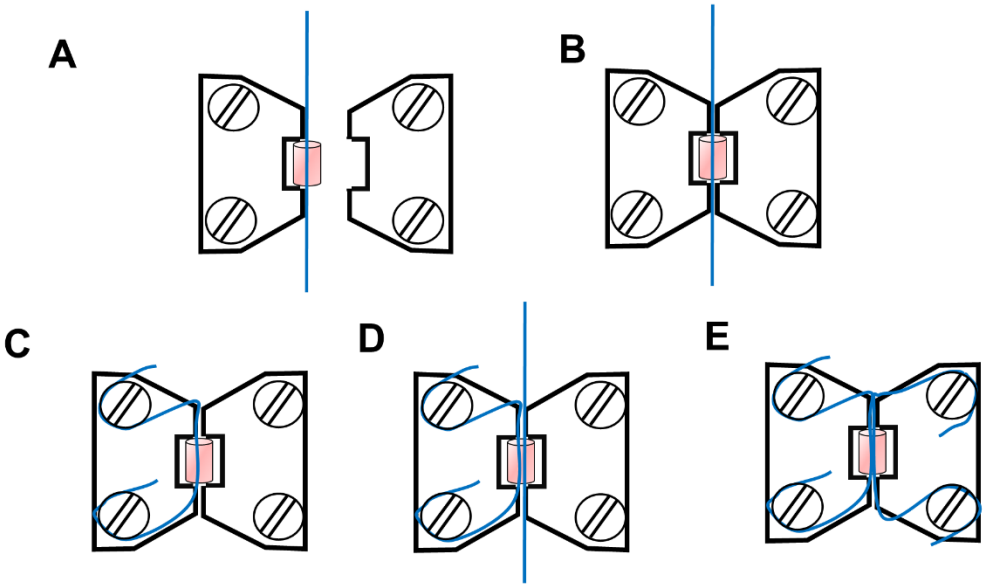

Figure 6. Schematic picture of the vessel mounting process

3.4.2. Separation wires and recording force (F)

1) Each ring was equilibrated for 5-10 min in PBS.
2) Starting from the completely unloaded state, the distance between the wires was gradually increased by manual adjustment of the micrometer. The distance between the wires was elongated by 0.05 mm each time.
3) This procedure was done until reaching the breaking point where the force

was no longer increased. The recording force was selected at the peak each time while changing the micrometer. The example is shown in Figure 7.

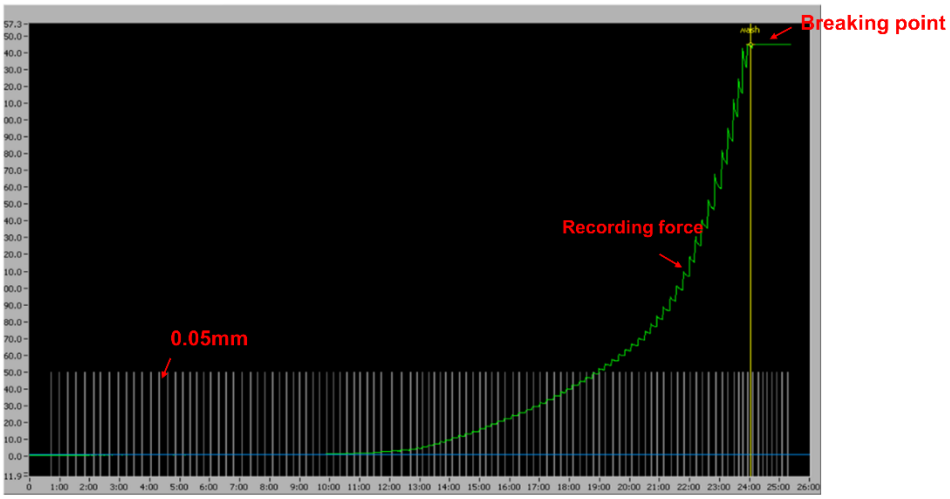

Figure 7. Representative picture of the SVM result. The recording force was selected at the peak each time while changing the micrometer. The distance between the wires was elongated by 0.05 mm each time. This procedure was done until reaching the breaking point where the force is no longer increased.

3.4.3. Measurement of the internal diameter of the ring (d), the diameter of the wire (Φ), the thickness of the ring (e_0), and the width of the ring (a_0)

1) After the SVM experiment, the ring was cut and its circumference (C) was measured by a ruler as shown in Figure 8. The internal diameter of the ring (d) = Circumference (C) / π.

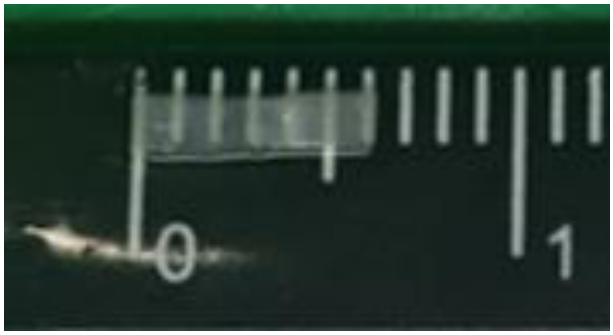

Figure 8. The picture of measuring the circumference of the ring by a ruler. The ring was cut and measured the circumference by a ruler after the SVM experiment. Circumference = 6 mm.

2) The diameter of the wire is 0.04 mm according to the user guideline [67].
3) The thickness of the ring was referenced in the previous article, thickness (e_0) = 0.08967 mm among 0-3 months [68].
4) The width of the ring (a_0) is around 2 mm.

3.4.4. Calculation of biomechanical properties

According to previous studies, five biomechanical parameters in the stress-stretch curve were summarized to represent the mechanical response of the arterial wall to simplify the analysis and allow comparisons [69-71]. The stress-stretch curve and the meaning of biomechanical properties are shown in Figure 9.

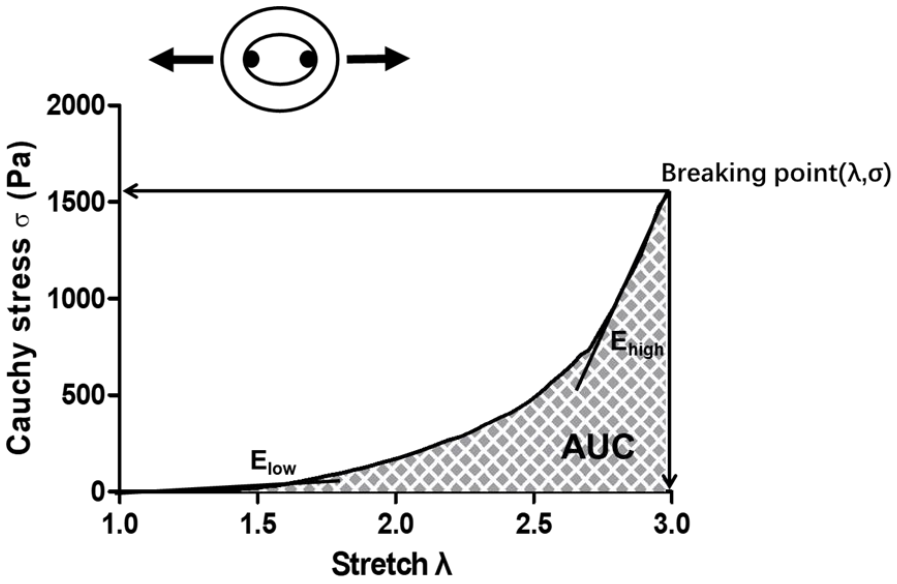

Figure 9. Stress-stretch curve and biomechanical properties. The stretch (λ, an index of deformation of the material), the Cauchy stress (σ, measurement of the internal force per unit of area). E_{low} and E_{high} are the modulus of the first and last 10% of the curve, respectively. AUC is the area under the stress-stretch curve. The breaking point is the point of the ring fracture ($\sigma_{breaking\ point}$ means the stress at the breaking point, $\lambda_{breaking\ point}$ means the stretch at the breaking point).

The expression of Cauchy stress (σ) was calculated by:

$$\sigma = \frac{F}{2a_0e_0}\lambda$$

Equation 3-1 Cauchy stress (σ). F: force; λ: stretch; a_0: ring width; e_0: ring thickness

The expression of stretch (λ) was defined by:

$$\lambda = 1 + 2\frac{(\Delta\text{-}\Delta_0)}{\pi d}$$

Equation 3-2 Stretch (λ). d: ring diameter; Δ_0: initial length that the ring starts to resist deformation; $\Delta\text{-}\Delta_0$: the elongation in the separation of the wires by manual adjustment of the micrometer every time

The initial length (Δ_0) was calculated by

$$\Delta_0 = \frac{\pi}{2}(\mathrm{d}\text{-}\phi)$$

Equation 3-3 Initial length (Δ_0). Δ_0: initial length that the ring starts to resist deformation; d: ring diameter; ϕ: wire diameter

The modulus of the first and last 10% of the stress-stretch curve was calculated as E_{low} and E_{high}. E_{low} represents the contribution of the elastin fiber to stiffness. E_{high} represents the contribution of the collagen fiber to stiffness.

The Area Under Curve (AUC) was calculated as the area under the stress-stretch curve, which means the energy absorbed by the ring.

The breaking point including breaking point_stress ($\sigma_{breaking\ point}$) and breaking point_stretch ($\lambda_{breaking\ point}$) is the maximum stress and maximum stretch in the stress-stretch curve. That means stress and stretch at breaking point.

3.5. Calcium content

The aortic rings were decalcified for 48 h in HCl on the thermomixer. The rings were then transferred into weighed reaction vessels. These rings were dried in a heated oven and weighed. The rings were homogenized, centrifuged at low speed, and supernatant was taken. The supernatant was concentrated in a

rotary vacuum concentrator. The residue, which contained the calcium dissolved in the aortas, was resuspended in HCl. Calcium content was quantified using the colorimetrical o-cresolphthalein method (Colorimetric Calcium Assay, SciencellTM, Berlin, Germany). After decalcification, cells were washed with phosphate-buffered saline (PBS) and lysed in 0.1 mol/l NaOH/0.1% SDS buffer. This forms a violet complex with calcium, which was measured photometrically at 570 nm after 15 minutes of incubation. The determined absolute calcium content was related to the dry weight of the respective aortic ring, whereby the relative calcium content of the aortic rings was determined in g/mg dry weight.

3.6. Statistical analysis

The experiments were conducted in at least three independent experiments to confirm the reproducibility of the results. Data were presented as means with mean± standard error (mean±SEM) unless otherwise indicated. Each dataset was tested for normal distribution using the Kolmogorov-Smirnov test. Datasets that did not pass this normality test were compared using the Mann-Whitney U test or Kruskal-Wallis-Test. Datasets that passed this normality test were compared using the T-test or One-way ANOVA. All data were analyzed using the GraphPad Prism software 5.0 (GraphPad Software Inc, La Jolla, CA, USA). The P-value < 0.05 was considered statistically significant.

4. Results

In the present study, five biomechanical parameters (E_{low}, E_{high}, AUC, $\sigma_{breaking\ point}$, and $\lambda_{breaking\ point}$) in the stress-stretch curve were calculated to represent the biomechanical properties of the arterial wall for simplified analysis and comparison, as shown in Figure 9.

In the first set of experiments, the basal (without stimulation) biomechanical properties and calcium content of the thoracic aorta were investigated. The second set of experiments investigated the biomechanical properties and calcium content in different regions of the thoracic aorta after 14 days CAM (Calcification medium) incubation. The conformity of different areas of the thoracic aorta is a prerequisite for follow-up experiments. Then, we analyzed the changes in biomechanical properties of the vessel wall during VC with two calcification inducers: high phosphate and Azathioprine.

4.1. Biomechanical properties and calcium content of the thoracic aortic wall: effect of location

4.1.1. Biomechanical properties and calcium content in different areas of the thoracic aorta without stimulation

To investigate biomechanical properties and calcium content in different areas of the thoracic aorta without stimulation. The thoracic aorta (removing the aortic arch) was cut into 18 rings that were numbered from the proximal to the distal end and were divided into P1, P2, M1, M2, D1, and D2. Biomechanical properties including E_{low}, E_{high}, AUC, $\sigma_{breaking\ point}$, and $\lambda_{breaking\ point}$ were calculated. Calcium content in different areas was also measured. In the comparison of biomechanical properties and calcium content in different areas of the thoracic aorta without stimulation, no significant differences were found. (see Figure 10 and Table 4-1)

Table 4-1. Biomechanical properties and calcium content in different areas of the thoracic aorta without stimulation (0 days). n=3 rats, each aorta 18 rings.

Parameter	P	*
E_{low}	0.5369	ns
E_{high}	0.3641	ns
AUC	0.7450	ns
$\sigma_{breaking\ point}$	0.6874	ns
$\lambda_{breaking\ point}$	0.2317	ns
Calcium content (µg/mg)	0.9698	ns

* < 0.05, ** < 0.01, *** < 0.001 and **** < 0.0001, ns > 0.05 compared with them based on Kruskal-Wallis-Test. Dunns comparisons were used as a post-test.

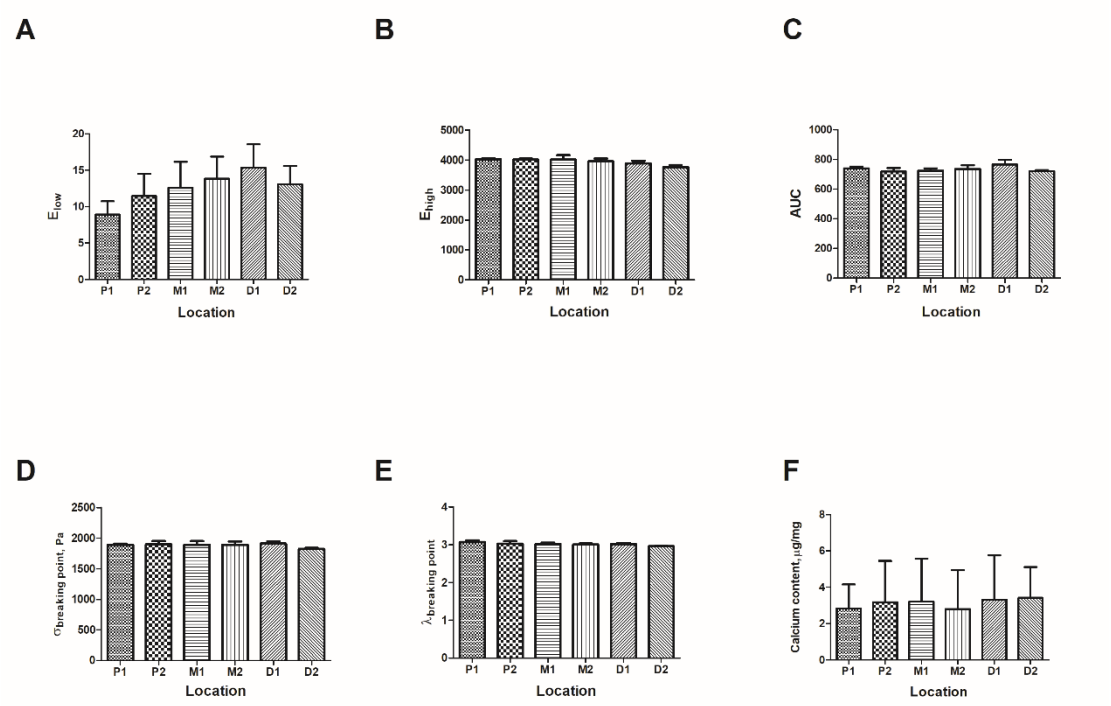

Figure 10. A-F: Comparison of biomechanical properties and calcium content in the different areas of the thoracic aorta without stimulation. The thoracic aorta was cut into 18 rings that were numbered from proximal to the distal end and were divided into P1, P2, M1, M2, D1, and D2. No significant differences were observed.

4.1.2. Biomechanical properties and calcium content in different areas of the thoracic aorta with calcification medium for 14 days

The thoracic aorta (removing the aortic arch) was cut into 18 rings around 2 mm. These rings were incubated with CAM (Calcification medium) for 14 days and were numbered from the proximal to the distal end and divided into P1, P2, M1, M2, D1, and D2. Biomechanical properties in different areas were calculated and calcium content was measured. Comparison of biomechanical

properties and calcium content in different areas of the thoracic aorta after 14 days CAM incubation, which demonstrated no statistically significant differences. (see Figure 11 and Table 4-2)

Table 4-2. Biomechanical properties and calcium content in different areas of the thoracic aorta after 14 days of treatment with CAM. n=3 rats, each aorta 18 rings.

Parameter	**P**	*
E_{low}	0.9369	ns
E_{high}	0.5236	ns
AUC	0.9962	ns
$\sigma_{breaking\ point}$	0.9909	ns
$\lambda_{breaking\ point}$	0.9988	ns
Calcium content (µg/mg)	0.9321	ns

* < 0.05, ** < 0.01, *** < 0.001 and **** < 0.0001, ns > 0.05 compared with them based on Kruskal-Wallis-Test. Dunns comparisons were used as a post-test.

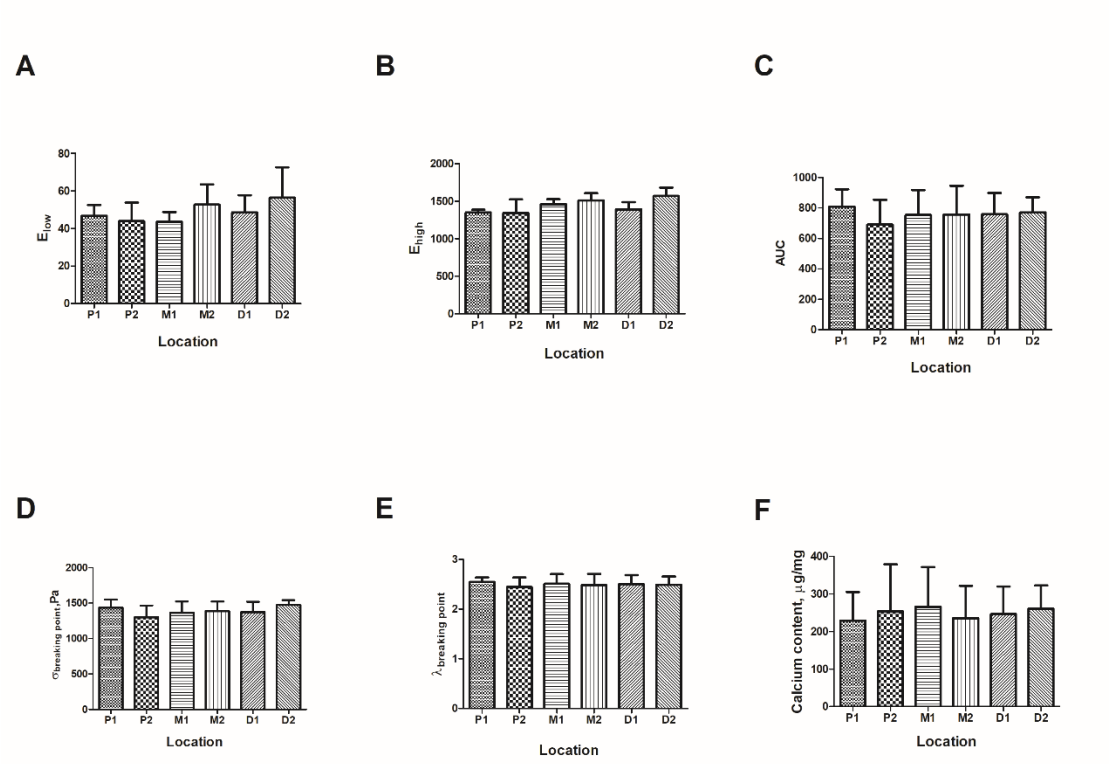

Figure 11. A-F: Comparison of biomechanical properties and calcium content in different areas of the thoracic aorta after 14 days CAM ex vivo incubation. The thoracic aorta was cut into 18 rings. These rings were numbered from proximal to the distal end and divided into P1, P2, M1, M2, D1, and D2. No statistically significant differences were observed.

4.2. The effect of phosphate on biomechanical properties and calcium content

To investigate how the duration of high phosphate ex vivo incubation affects biomechanical properties and calcium content, these rings were incubated with CAM (Calcification medium) and COM (Control medium) ex vivo and harvested at different time points. While comparing biomechanical properties between CAM and COM, E_{high} and calcium content had significant differences between CAM and COM, whereas other biomechanical properties had no significant differences after 3 days (see Figure 12).

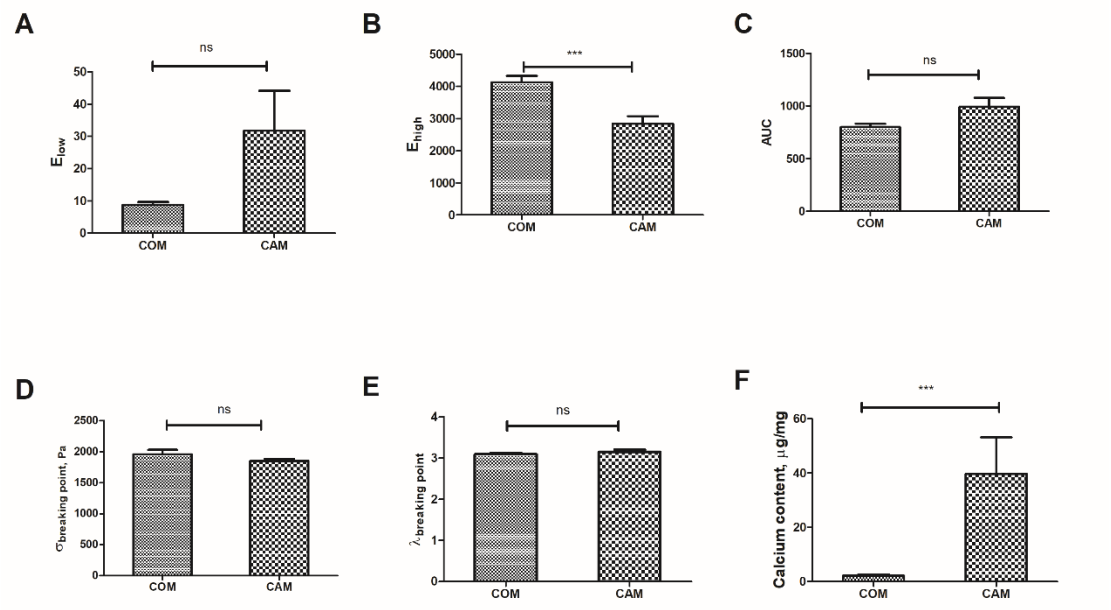

Figure 12. A-F: Comparison of biomechanical properties and calcium content between CAM and COM at 3 days (N≥6). E_{high} and calcium content had significant differences between CAM and COM. Other biomechanical properties including E_{low}, $\sigma_{breaking\ point}$, $\lambda_{breaking\ point}$, AUC had no significant differences between CAM and COM. * < 0.05, ** < 0.01, *** < 0.001 and **** < 0.0001, ns > 0.05. Statistically significant differences were tested with T-test or Mann-Whitney-U test.

After 7 days, the data indicated that E_{low}, E_{high} $\sigma_{breaking\ point}$, $\lambda_{breaking\ point}$, and calcium content had significant differences between CAM and COM, while AUC had no significant difference between CAM and COM. We observed that E_{low} and calcium content had the significant increase, whereas E_{high}, $\sigma_{breaking\ point}$,

and $\lambda_{breaking\ point}$ had the significant decrease (Figure 13)

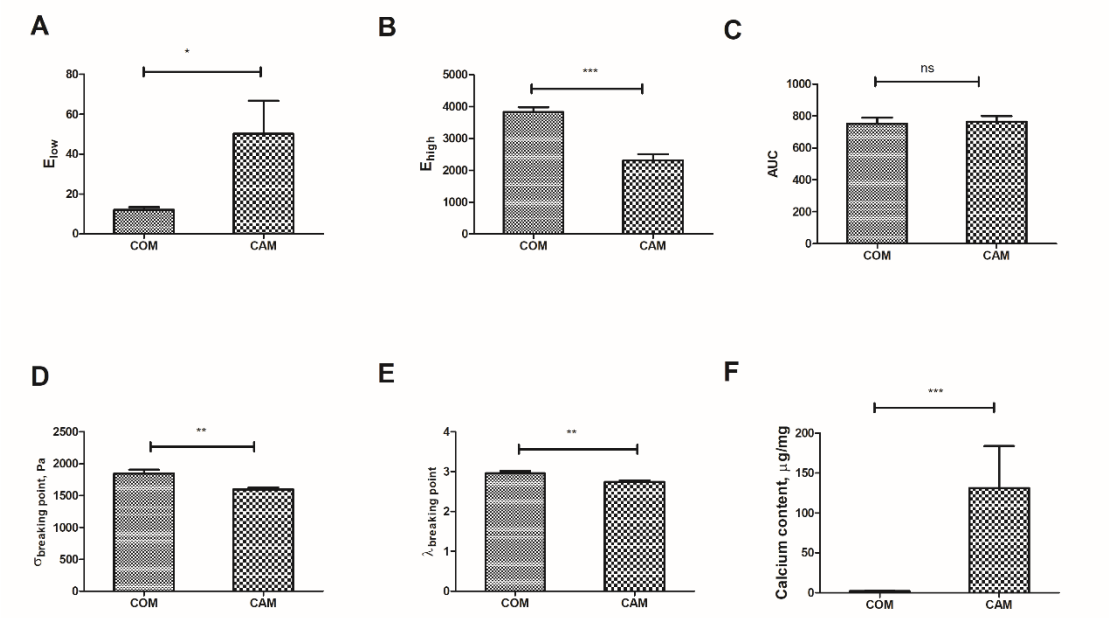

Figure 13. A-F: Comparison of biomechanical properties and calcium content between CAM and COM at 7 days (N≥6). E_{low}, E_{high}, $\sigma_{breaking\ point}$, $\lambda_{breaking\ point}$, and calcium content had significant differences between CAM and COM, while AUC had no significant difference between CAM and COM. * < 0.05, ** < 0.01, *** < 0.001 and **** < 0.0001, ns > 0.05. Statistically significant differences were tested with T-test or Mann-Whitney-U test.

After 14 days, the results showed that E_{low}, E_{high} $\sigma_{breaking\ point}$, $\lambda_{breaking\ point}$, and calcium content differed significantly between CAM and COM, while AUC had no significant differences between CAM and COM (see Figure 14).

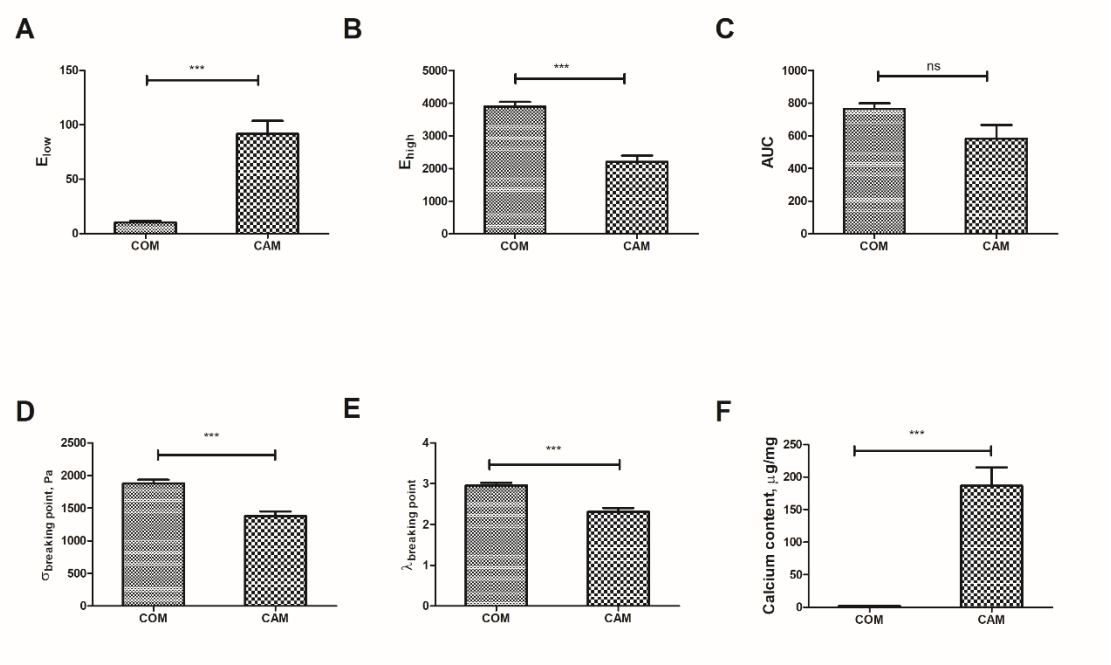

Figure 14. A-F: Comparison of biomechanical properties and calcium content between CAM and COM at 14 days (N≥6). E_{low}, E_{high}, $\sigma_{breaking\ point}$, $\lambda_{breaking\ point}$, and calcium content differed significantly between CAM and COM, while AUC had no significant difference between CAM and COM. * < 0.05, ** < 0.01, *** < 0.001 and **** < 0.0001, ns > 0.05. Statistically significant differences were tested with T-test or Mann-Whitney-U test.

After 21 days, significant differences in calcium content and biomechanical properties including E_{low}, E_{high}, $\sigma_{breaking\ point}$, and $\lambda_{breaking\ point}$ were found, yet no significant difference in AUC was found between CAM and COM (see Figure 15).

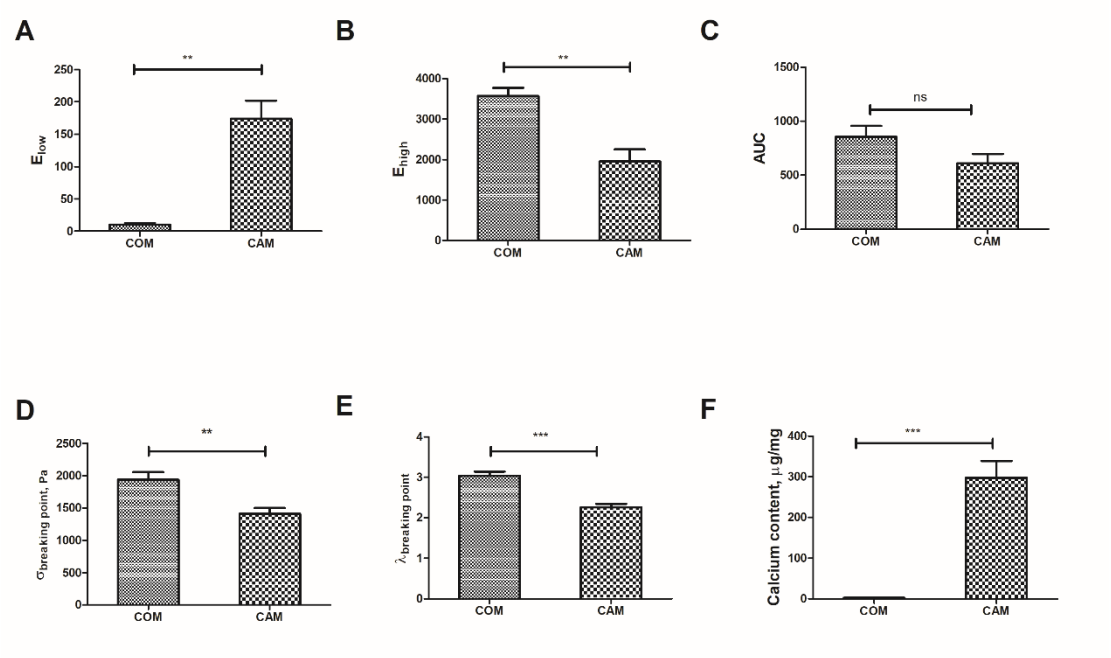

Figure 15. A-F: Comparison of biomechanical properties and calcium content between CAM and COM at 21 days (N≥6). Calcium content, E_{low}, E_{high}, $\sigma_{breaking\ point}$, and $\lambda_{breaking\ point}$ differed significantly between CAM and COM. * < 0.05, ** < 0.01, *** < 0.001 and **** < 0.0001, ns > 0.05. Statistically significant differences were tested with T-test or Mann-Whitney-U test.

4.3. The effect of Azathioprine on biomechanical properties and calcium content

There is an increasing body of indirect and direct evidence that immunosuppressive therapy may have an effect on the progression of VC [57]. Azathioprine (AZA) is an immunosuppressive drug, which is routinely used to treat several auto-immune diseases and after organ transplantation [72, 73]. Our previous studies have shown that AZA and 6-MP (its cleavage product) can induce VC both in vivo and ex vivo [59, 60]. Therefore, in this study, we used AZA as the calcification inducer to investigate how the duration of AZA ex vivo incubation affects biomechanical properties and calcium content. The rings were incubated with CAM+AZA, CAM, COM, and COM+AZA and harvested at different time points. Biomechanical properties and calcium content showed no statistical difference between CAM+AZA and CAM at 3 days (see Figure 16). At 7 days, significant differences in biomechanical properties including $\lambda_{breaking}$

$_{point}$ and AUC were observed between CAM+AZA and CAM, whereas E_{low}, E_{high}, $\sigma_{breaking\ point}$, and calcium content had no significant differences between CAM+AZA and CAM (see Figure 17). After 14 days, significant differences in E_{low}, $\lambda_{breaking\ point}$, AUC, and calcium content were found between CAM+AZA and CAM (see Figure 18). After 21 days, the data indicated that E_{low}, and calcium content had significant differences between CAM+AZA and CAM, but other biomechanical properties had no significant differences between CAM+AZA and CAM (Figure 19). When comparing COM+AZA and COM, there were no significant differences in biomechanical properties and calcium content at 3, 7, 14, and 21 days, respectively (Figure 16, Figure 17, Figure 18, and Figure 19).

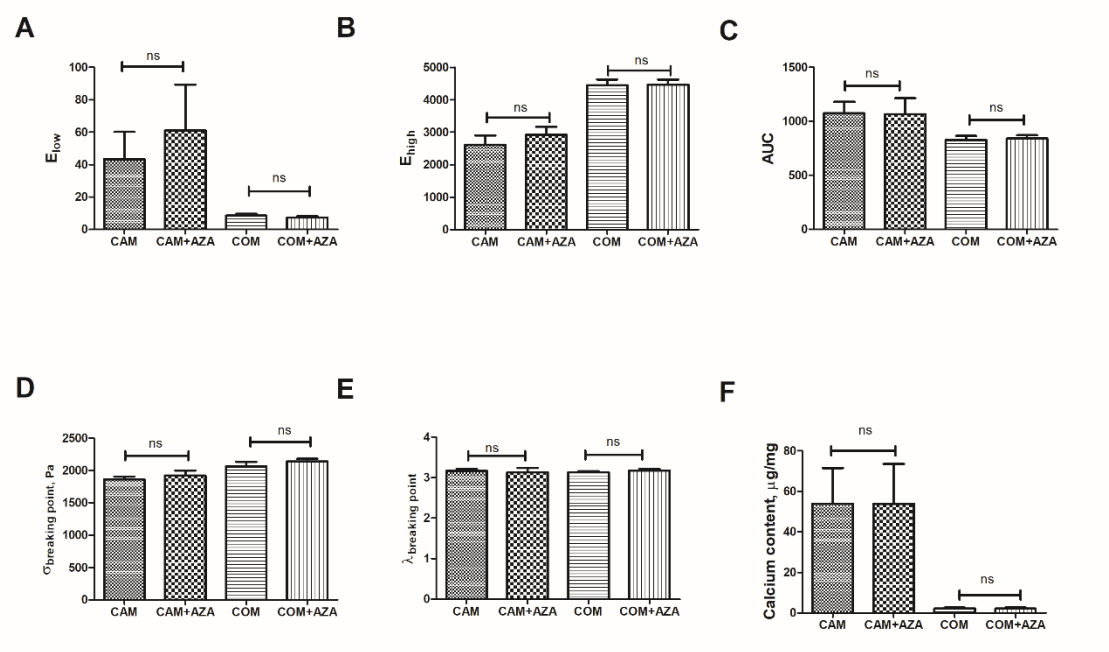

Figure 16. A-F: Comparison of biomechanical properties and calcium content in CAM +AZA, CAM, COM, and COM+AZA at 3 days (N≥6). No significant differences in calcium content and biomechanical properties were observed. * < 0.05, ** < 0.01, *** < 0.001 and **** < 0.0001, ns > 0.05 compared with them based on one-way ANOVA. Bonferroni's multiple comparisons were used as a post-test.

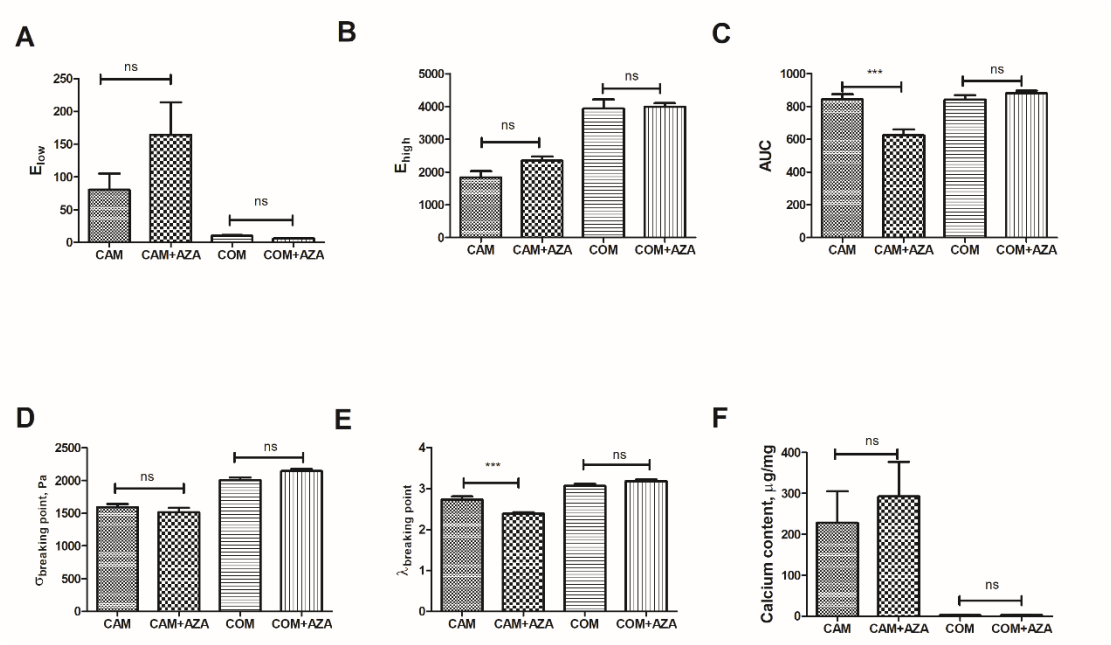

Figure 17. A-F: Comparison of biomechanical properties and calcium content in CAM+AZA, CAM, COM, and COM+AZA at 7 days (N≥6). Significant differences in $\lambda_{breaking\ point}$ and AUC were observed between CAM+AZA and CAM. Calcium content and biomechanical properties had no significant differences between COM and COM+AZA. * < 0.05, ** < 0.01, *** < 0.001 and **** < 0.0001, ns > 0.05 compared with them based on one-way ANOVA. Bonferroni's multiple comparisons were used as a post-test.

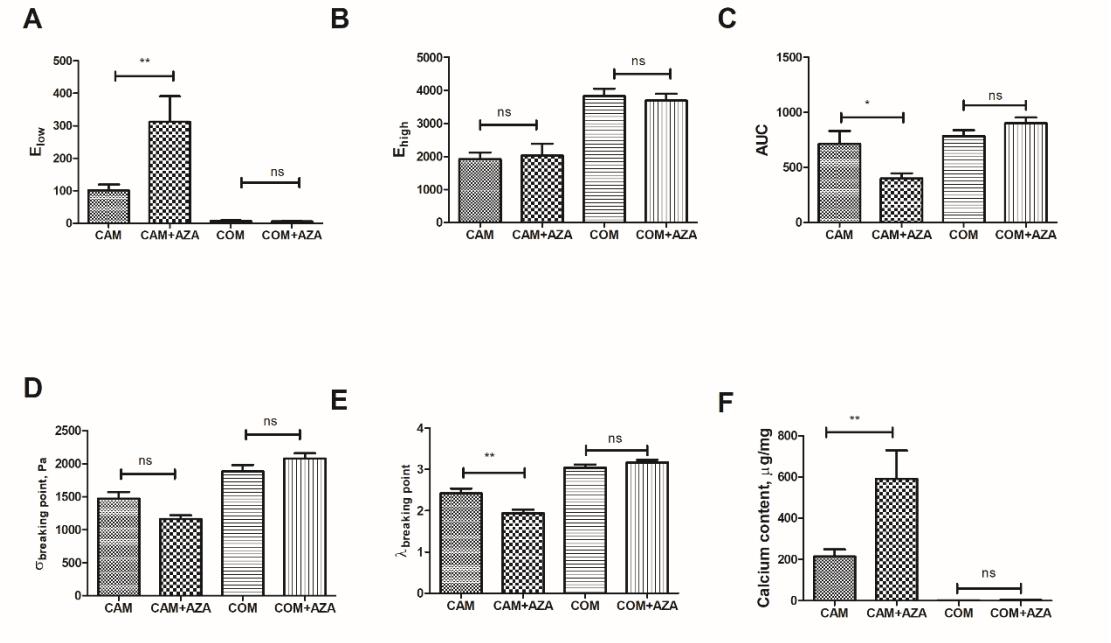

Figure 18. A-F: Comparison of biomechanical properties and calcium content in CAM+AZA, CAM, COM, and COM+AZA at 14 days (N≥6). Significant differences in E_{low}, $\lambda_{breaking\ point}$, AUC, and calcium content were found between CAM+AZA and CAM. Calcium content and biomechanical properties had no significant differences between COM and COM+AZA. * <

0.05, ** < 0.01, *** < 0.001 and **** < 0.0001, ns > 0.05 compared with them based on one-way ANOVA. Bonferroni's multiple comparisons were used as a post-test.

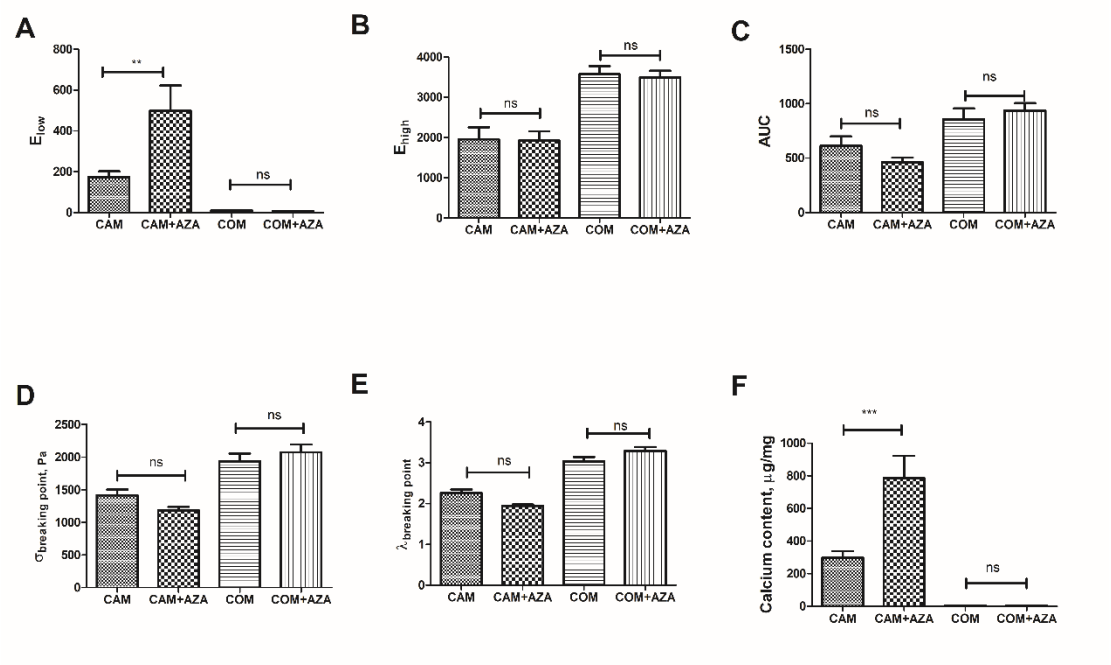

Figure 19. A-F: Comparison of biomechanical properties and calcium content in CAM+AZA, CAM, COM, and COM+AZA at 21 days (N≥6). Significant differences in E_{low} and calcium content were observed between CAM+AZA and CAM. * < 0.05, ** < 0.01, *** < 0.001 and **** < 0.0001, ns > 0.05 compared with them based on one-way ANOVA. Bonferroni's multiple comparisons were used as a post-test.

Summary of results

- High phosphate can affect biomechanical properties during vascular calcification, which is related to incubation time.
- AZA can affect biomechanical properties during vascular calcification, which is relevant to incubation time. However, this effect requires the presence of high phosphate.

5. Discussion

The wall of the vessel is composed of cells and the specialized extracellular matrix that provides unique biomechanical properties. As a result of ectopic calcium phosphate mineral deposition (calcification), the vascular walls are damaged and remodeled, which changes the biomechanical properties of the vessels. The correlation between VC and biomechanical properties has already been shown in humans and animals [74]. Currently, several methods have been established for the assessment of vascular calcification. They include not only the direct detection of calcium, phosphate, and hydroxyapatite deposition by biochemical, histological staining, and specialized preclinical imaging methods, but also the detection of biochemical markers of pathological calcification and functional markers of vessels [61].

In contrast to other methods, the functional biomechanical parameters of vessels can represent changes in biomechanical properties and help better understand the disruption of the media, advanced remodeling processes of the vessel wall, and changes in arterial wall stiffness during VC. However, research in this field is still limited. In this study, we established a method to investigate biomechanical properties in the process of VC in an ex vivo setting and indicated changes in biomechanical properties with the incubation time of calcification inducers.

5.1. Impact of high phosphate on biomechanical properties during vascular calcification

Phosphate plays an important role in the development and aggravation of vascular calcifications. A misbalance of phosphate metabolism plays a crucial role in the progression of VC [75, 76]. The phosphate level in the serum is maintained within the normal range by balancing extracellular phosphate with phosphate in intracellular fluid or bone, intestinal phosphate absorption, and renal tubular phosphate reabsorption. In CKD patients, renal phosphate filtration and reabsorption are impaired, thus disrupting the homeostasis of

serum phosphate levels. It is noteworthy that the progression of VC in CKD depends on time, whereas VC in ESRD patients is more common [77]. In previous studies, researchers systematically explored the effect of phosphate concentration on calcium content in ex vivo settings [78, 79]. However, studies on the effect of phosphate on biomechanical properties during VC are lacking in the main literature. In my study, I not only investigated the effect of phosphate on calcium content but also analyzed the effect of phosphate on biomechanical properties using the passive mechanical response experiment.

The passive mechanical response of artery walls is mainly due to elastic fibers and collagen fibers [80]. The influence of VC on biomechanical properties is mainly due to elastic fibers and collagen fibers. Selective digestion of elastic fibers or collagen fibers with proteases demonstrated that the elastic fibers are resistant to stretch at low pressures, while the collagen fibers are resistant to stretch at high pressures [81, 82]. Experiments have indicated the circumferential material stiffness at low pressure will decrease in the aorta of mice lacking elastin ($Eln^{-/-}$), in line with the observed role of elastic fibers in protease experiments [83]. The material properties of the arterial wall are nonlinear and vary with the direction of loading and deformation. Evaluation of the material properties of the arterial wall can be obtained by the mechanical response within a given deformation or loading range in a specified direction to provide an incremental Young's modulus for comparison [84]. According to the principle of physics and previous articles, the assessment of E_{low} and E_{high} was performed by taking the small modulus between 5% to 20% for uniaxial cases and 10% to 25% for ring tests [22, 70, 85].

In my research, E_{low} (the modulus of the first 10% of the stress-stretch curve) means that the elastin substance contributes to stiffness. Compared to COM (Control medium), increasing E_{low} represents elastin destruction or degradation with CAM (Calcification medium) incubation (shown in Figure 12, Figure 13, Figure 14, and Figure 15). Elastin, the matrix protein responsible for reversible

elasticity, provides the necessary elasticity of the artery for proper cardiovascular function. Many cardiovascular diseases are associated with disorganization or inadequacy, inappropriate assembly, biochemical modifications, and fragmentation of elastic fibers [80, 86, 87]. The correlation between elastin degradation and VC has not been fully elucidated. Initial phases of calcification appeared to be related to persistent elastin degradation. Elastin comprises neutral or uncharged binding sites that have a powerful affinity to positive calcium ions. In a normal situation, calcification can be prevented via glycoproteins like fibrillins and fibulins surrounding the elastin. Under pathological conditions, the loss of these elastin coatings allows amorphous elastin to bind to calcium, which is positively charged due to binding calcium ions, attracting charge-neutralizing carbonate and phosphate ions, further binding calcium ions – which is an iterative process. Therefore, degraded elastin can provide a nidus for calcium-binding and can further exacerbate calcification [88-90]. Fibrillin deficient mice showed the degradation of elastic fiber and severe medial calcification in the artery [91]. Microfibril-associated glycoprotein (MAGP) knockout mice will die because of acute calcification in the arterial elastic layer leading to rupture of the thoracic or abdominal aorta within 2 months [92]. In addition, some elastases and elastolytic enzymes that cleave soluble and insoluble elastin will also increase during the process of elastin degradation. These enzymes, which include serine and cysteine cathepsins-L, K, S, and V (Cat L, K, S, and V), and matrix metalloproteinases-2, 7, 9, and 12 (MMP-2, -7, -9, and -12), are important in the degradation of elastic fibers, which affects vascular calcification. Several studies indicated a correlation between MMP-mediated elastin degradation and VC, especially MMP-2 and MMP-9 [93-95]. Dina M. Basalyga, M.S. et al. demonstrated that the rat abdominal aorta with low concentrations of calcium chloride ($CaCl_2$) induced high expression of MMP-9 and MMP-2 to mediate chronic aortic degeneration and calcification of vascular elastic fibers. However,

there was no elastin calcification in both MMP-2 and MMP-9 deficient mice with the same $CaCl_2$ treatment [96]. Cysteine cathepsins are another kind of the most potent elastases. Aikawa et al. found that calcification is increased in the chronic renal disease (CRD) $apoE^{-/-}/CatS^{+/+}$ cohort, whereas CRD $apoE^{-/-}/CatS^{-/-}$ mice showed less inflammation and calcification. Additionally, recombinant CatS significantly increased calcification in SMC, which was further amplified in the phosphate-enriched culture medium [97]. Another study by Andrault et al. indicated that degradation of elastin by CatK, S, and V directly accelerates elastin calcification by the generation of nidus in the extracellular matrix, and cathepsin-generated elastin peptides can cause the phenotypic change in SMC osteoblast and cellular calcification [98].

In my study, E_{high} (the modulus of the last 10% in the stress-stretch curve) means that collagen substance contributes to stiffness, which is gradually decreased representing collagen deposition and accumulation. In comparison to COM (Control medium), decreasing E_{high} represents collagen deposition and accumulation with CAM (Calcification medium) incubation (shown in Figure 12, Figure 13, Figure 14, and Figure 15). Collagen molecules are composed of unique triple helix structures, which are primarily produced by osteoblasts, chondroblasts, and fibroblasts [99]. The generation of mature collagen fiber is a very complex process that involves gene transcription, posttranslational modification, and extracellular excretion and is regulated by the various organelles and biological molecules [32]. Under a pathological situation, the quality or quantity of collagen will change due to a disturbance of the balance between collagen synthesis and degradation, whichultimately triggers diseases [100-102]. Collagen I and III are the main components of the vascular matrix, comprising 60% and 30% of total vascular collagen, respectively. And their relative levels remain stable under physiological situations [103]. The expression of type I collagen (Col1) marks the extracellular matrix maturation that was obviously increased during VC [38]. Meanwhile, abnormal collagen

can also affect the metabolism of calcification inhibitors like inorganic pyrophosphate (PPi). PPi is an important calcification inhibitor [104]. On the one hand, excessive collagen reduces PPi synthesis by downregulating the expression of ectonucleotide pyrophosphatase/phosphodiesterase 1 (ENPP1) which is the key to PPi maturation [105]. On the other hand, collagen can promote the hydrolysis of PPi by increasing the tissue nonspecific alkaline phosphatase (TNAP) activity of vascular smooth muscle cell-derived matrix vesicles (VSMC-MVs) [106]. The synthesis of PPi is decreased, and PPi hydrolysis is increased, which facilitates the occurrence of VC. Recently, evidence indicated that phosphate regulation-related drugs for CKD patients have the potential to ameliorate VC by inhibiting the expression of collagen. Cinacalcet inhibits the secretion of collagen I to alleviate the VC process by activating calcium-sensing receptors of VSMCs [107]. Lanthanum carbonate was also effective in decreasing the expression of collagen I to regress VC in mouse models [108]. The treatment abolishes the effect of aberrant collagen without affecting the biological function of normal collagen and will become a new therapy for VC.

In my research, breaking point_stress ($\sigma_{breaking\ point}$) and breaking point_stretch ($\lambda_{breaking\ point}$) mean the stress and the stretch at the breaking point. Compared to COM (Control medium), decreasing $\sigma_{breaking\ point}$ and $\lambda_{breaking\ point}$ suggested that rings were easy to break with CAM (Calcification medium) incubation. (shown in Figure 12, Figure 13, Figure 14, and Figure 15). This might explain why calcified vessels are prone to rupture.

5.2. Impact of AZA on biomechanical properties during vascular calcification

AZA is used as an immunosuppressant for the treatment of several auto-immune diseases and organic transplantation in clinical practice. Our previous study already demonstrated that AZA and 6-MP (its cleavage product) are VC inducers. The generation of reactive oxygen specifies (ROS) by 6-MP could be

responsible for the transdifferentiation of VSMCs, which stimulated the transdifferentiation of VSMCs into an osteo-chondrogenic cell (OCC) phenotype. This effect could also be verified by measurement of the calcium deposition and enzyme activity of alkaline phosphatase (ALP), and the expression levels of some critical proteins-like cbfa1 and osteocalcin (OCN) [59]. Cbfa1, alternatively referred to as Runx2, is a crucial transcription factor in osteoblastic differentiation, which drives the primary osteoblastic differentiation factor of VSMCs that is essential for medial calcification among mice [109, 110]. OCN is not only used as an osteoblast-specific intracellular marker but is also a late marker of differentiation and increases as the mineral is deposited [111, 112]. In addition, in our recent study, we investigated the long-term effect of AZA treatment on mVC in rats, which induces calcification and proinflammatory senescence-associated secretory phenotype (SASP) activation in the artery. SASP cytokines (mainly IL-1β and IL-6) increased significantly with AZA treatment. IL-1β and IL-6 are both known as inducers of mineralization in VSMC [113-115]. IL-6 induced calcification of VSMC and upregulated the expressions of bone morphogenetic protein 2 (BMP2), osteoprotegerin (OPG), and osteopontin (OPN) in vitro [116]. After AZA treatment, these proteins mentioned above are upregulated in the aortic rings [60]. For IL-1β, the effect is associated with the NLR family pyrin domain containing 3 (NLRP3) inflammasome, and 6-shogaol can alleviate calcification of human artery smooth muscle cells via inhibiting NLRP3 inflammasome [117]. The area of medial VC and calcium content significantly increased with AZA treatment in the aortic rings of $NLRP3^{+/+}$ mice. However, in $NLRP3^{-/-}$ mice, the induction impact of AZA is significantly reduced [60].

In this study, we used AZA as the calcification inducer and examined how AZA affects biomechanical properties during VC. E_{low} was higher in the CAM+AZA group as compared with the CAM group at 14 and 21 days (shown in Figure 16, Figure 17, Figure 18, and Figure 19). The exact cause is unknown, but it could

be related to AZA and its metabolites, which activate proinflammatory cytokines like IL-1β, and IL-6 [59]. Some of these proinflammatory cytokines damage the elastic protein and lead to artery remodeling. Low-level inflammation is well accepted as a major contributor to the small-sized muscular artery and large elastic artery remodeling [118, 119]. Interestingly, when comparing COM+AZA with the COM group, biomechanical properties and calcium content had no significant differences (shown in Figure 16, Figure 17, Figure 18, and Figure 19). The results may indicate that the effect of AZA demands the presence of high phosphate. That also deserves our attention.

6. Conclusion

In this study, a protocol for the detection of biomechanical properties of the vessel wall during vascular calcification was established and validated. This protocol expands the current analytical tools in the research field of VC, which can directly describe changes in vascular biomechanical properties during VC. This method can provide specified information on the mechanical role of collagen and elastin networks and help better understand the disruption of the media, advanced remodeling processes of the vessel wall, and stiffness changes in the arterial wall during VC.

7. References

1. Collaborators, G.B.D.R.F., Global, regional, and national comparative risk assessment of 79 behavioural, environmental and occupational, and metabolic risks or clusters of risks, 1990-2015: a systematic analysis for the Global Burden of Disease Study 2015. Lancet, 2016. **388**(10053): p. 1659-1724.

2. Voelkl, J., D. Cejka, and I. Alesutan, An overview of the mechanisms in vascular calcification during chronic kidney disease. Curr Opin Nephrol Hypertens, 2019. **28**(4): p. 289-296.

3. Mönckeberg, J., VIII. Über die reine Mediaverkalkung der Extremitätenarterien und ihr Verhalten zur Arteriosklerose.(Aus dem Pathologisch-anatomischen Institut des Allgem. Krankenhauses Hainburg-Eppendorf.), in Band 171. 1903, De Gruyter. p. 141-167.

4. Otsuka, F., K. Sakakura, K. Yahagi, M. Joner, and R. Virmani, Has our understanding of calcification in human coronary atherosclerosis progressed? Arterioscler Thromb Vasc Biol, 2014. **34**(4): p. 724-36.

5. Marchand, F. Über arteriosklerose (athero-sklerose). in Verhandlungen des Kongress für innere medizin. 1904.

6. Leopold, J.A., Vascular calcification: Mechanisms of vascular smooth muscle cell calcification. Trends Cardiovasc Med, 2015. **25**(4): p. 267-74.

7. Lanzer, P., F.M. Hannan, J.D. Lanzer, J. Janzen, P. Raggi, D. Furniss, M. Schuchardt, R. Thakker, P.-W. Fok, and J. Saez-Rodriguez, Medial arterial calcification: JACC state-of-the-art review. Journal of the American College of Cardiology, 2021. **78**(11): p. 1145-1165.

8. Lanzer, P., M. Boehm, V. Sorribas, M. Thiriet, J. Janzen, T. Zeller, C. St Hilaire, and C. Shanahan, Medial vascular calcification revisited: review and perspectives. Eur Heart J, 2014. **35**(23): p. 1515-25.

9. Cozzolino, M., P. Ciceri, A. Galassi, M. Mangano, S. Carugo, I. Capelli, and G. Cianciolo, The Key Role of Phosphate on Vascular Calcification. Toxins (Basel), 2019. **11**(4).

10. Johnson, R.C., J.A. Leopold, and J. Loscalzo, Vascular calcification: pathobiological mechanisms and clinical implications. Circ Res, 2006. **99**(10): p. 1044-59.

11. Wilson, P.W., L.I. Kauppila, C.J. O'Donnell, D.P. Kiel, M. Hannan, J.M. Polak, and L.A. Cupples, Abdominal aortic calcific deposits are an important predictor of vascular morbidity and mortality. Circulation, 2001. **103**(11): p. 1529-34.

12. Shaw, L.J., A.E. Giambrone, M.J. Blaha, J.T. Knapper, D.S. Berman, N. Bellam, A. Quyyumi, M.J. Budoff, T.Q. Callister, and J.K. Min, Long-Term Prognosis After Coronary Artery Calcification Testing in Asymptomatic Patients: A Cohort Study. Ann Intern Med, 2015. **163**(1): p. 14-21.

13. Budoff, M., J.C. Backlund, D.A. Bluemke, J. Polak, I. Bebu, D. Schade, S. Strowig, P. Raskin, J.M. Lachin, and D.E.R. Group, The Association of Coronary Artery Calcification With Subsequent Incidence of Cardiovascular Disease in Type 1 Diabetes: The DCCT/EDIC Trials. JACC Cardiovasc Imaging, 2019. **12**(7 Pt 2): p. 1341-1349.

14. Lioufas, N.M., E. Pedagogos, C.M. Hawley, E.M. Pascoe, G.J. Elder, S.V. Badve, A. Valks, N.D. Toussaint, and I.-C.K.D.I. on behalf of the, Aortic Calcification and Arterial Stiffness Burden in a Chronic Kidney Disease Cohort with High Cardiovascular Risk: Baseline Characteristics of the Impact of Phosphate Reduction On Vascular End-Points in Chronic Kidney Disease Trial. Am J Nephrol, 2020. **51**(3): p. 201-215.

15. Russo, D., S. Corrao, Y. Battaglia, M. Andreucci, A. Caiazza, A. Carlomagno, M. Lamberti, N. Pezone, A. Pota, L. Russo, M. Sacco, and B. Scognamiglio, Progression of coronary artery calcification and cardiac events in patients with chronic renal disease not receiving dialysis. Kidney Int, 2011. **80**(1): p. 112-8.

16. Blacher, J., A.P. Guerin, B. Pannier, S.J. Marchais, and G.M. London, Arterial calcifications, arterial stiffness, and cardiovascular risk in end-stage

renal disease. Hypertension, 2001. **38**(4): p. 938-42.

17. Goodman, W.G., J. Goldin, B.D. Kuizon, C. Yoon, B. Gales, D. Sider, Y. Wang, J. Chung, A. Emerick, L. Greaser, R.M. Elashoff, and I.B. Salusky, Coronary-artery calcification in young adults with end-stage renal disease who are undergoing dialysis. N Engl J Med, 2000. **342**(20): p. 1478-83.

18. Singh, C., C.S. Wong, and X. Wang, Medical Textiles as Vascular Implants and Their Success to Mimic Natural Arteries. J Funct Biomater, 2015. **6**(3): p. 500-25.

19. Thubrikar, M.J., Vascular mechanics and pathology. Vol. 494. 2007: Springer.

20. Wagenseil, J.E. and R.P. Mecham, Vascular extracellular matrix and arterial mechanics. Physiol Rev, 2009. **89**(3): p. 957-89.

21. Lee, R.T. and R.D. Kamm, Vascular mechanics for the cardiologist. J Am Coll Cardiol, 1994. **23**(6): p. 1289-95.

22. Camasao, D.B. and D. Mantovani, The mechanical characterization of blood vessels and their substitutes in the continuous quest for physiological-relevant performances. A critical review. Mater Today Bio, 2021. **10**: p. 100106.

23. Kozel, B.A. and R.P. Mecham, Elastic fiber ultrastructure and assembly. Matrix Biol, 2019. **84**: p. 31-40.

24. Etchevers, H.C., C. Vincent, N.M. Le Douarin, and G.F. Couly, The cephalic neural crest provides pericytes and smooth muscle cells to all blood vessels of the face and forebrain. Development, 2001. **128**(7): p. 1059-68.

25. Molinari-Tosatti, M.P., L. Galzigna, V. Moret, and L. Gotte, Some features of the binding of calcium ions to elastin. Calcif Tissue Res, 1968: p. Suppl:88.

26. Yu, S.Y. and H.T. Blumenthal, The calcification of elastic fibers. I. Biochemical studies. J Gerontol, 1963. **18**: p. 119-26.

27. Schiffmann, E., D.R. Lavender, E.J. Miller, and B.A. Corcoran, Amino acids at the nucleating site in mineralizing elastic tissue. Calcif Tissue Res, 1969. **3**(2): p. 125-35.

28. Contri, M.B., F. Boraldi, F. Taparelli, A. De Paepe, and I.P. Ronchetti, Matrix proteins with high affinity for calcium ions are associated with mineralization within the elastic fibers of pseudoxanthoma elasticum dermis. Am J Pathol, 1996. **148**(2): p. 569-77.

29. Gheduzzi, D., F. Boraldi, G. Annovi, C.P. DeVincenzi, L.J. Schurgers, C. Vermeer, D. Quaglino, and I.P. Ronchetti, Matrix Gla protein is involved in elastic fiber calcification in the dermis of pseudoxanthoma elasticum patients. Lab Invest, 2007. **87**(10): p. 998-1008.

30. Fornieri, C., M. Baccarani-Contri, D. Quaglino, Jr., and I. Pasquali-Ronchetti, Lysyl oxidase activity and elastin/glycosaminoglycan interactions in growing chick and rat aortas. J Cell Biol, 1987. **105**(3): p. 1463-9.

31. Fornieri, C., F. Taparelli, D. Quaglino, Jr., M.B. Contri, J.M. Davidson, S. Algeri, and I.P. Ronchetti, The effect of caloric restriction on the aortic tissue of aging rats. Connect Tissue Res, 1999. **40**(2): p. 131-43.

32. Ricard-Blum, S., The collagen family. Cold Spring Harb Perspect Biol, 2011. **3**(1): p. a004978.

33. Osidak, M.S., E.O. Osidak, M.A. Akhmanova, S.P. Domogatsky, and A.S. Domogatskaya, Fibrillar, fibril-associated and basement membrane collagens of the arterial wall: architecture, elasticity and remodeling under stress. Curr Pharm Des, 2015. **21**(9): p. 1124-33.

34. Hodroge, A., E. Trecherel, M. Cornu, W. Darwiche, A. Mansour, K. Ait-Mohand, T. Verissimo, C. Gomila, C. Schembri, S. Da Nascimento, R. Elboutachfaiti, A. Boullier, E. Lorne, J. Courtois, E. Petit, S. Toumieux, J. Kovensky, P. Sonnet, Z.A. Massy, S. Kamel, C. Rossi, and J. Ausseil, Oligogalacturonic Acid Inhibits Vascular Calcification by Two Mechanisms: Inhibition of Vascular Smooth Muscle Cell Osteogenic Conversion and Interaction With Collagen. Arterioscler Thromb Vasc Biol, 2017. **37**(7): p. 1391-1401.

35. Jover, E., A. Silvente, F. Marin, J. Martinez-Gonzalez, M. Orriols, C.M.

Martinez, C.M. Puche, M. Valdes, C. Rodriguez, and D. Hernandez-Romero, Inhibition of enzymes involved in collagen cross-linking reduces vascular smooth muscle cell calcification. FASEB J, 2018. **32**(8): p. 4459-4469.

36. Bai, Y., J. Zhang, J. Xu, L. Cui, H. Zhang, and S. Zhang, Alteration of type I collagen in the radial artery of patients with end-stage renal disease. Am J Med Sci, 2015. **349**(4): p. 292-7.

37. Freise, C., V. Bobb, and U. Querfeld, Collagen XIV and a related recombinant fragment protect human vascular smooth muscle cells from calcium-/phosphate-induced osteochondrocytic transdifferentiation. Exp Cell Res, 2017. **358**(2): p. 242-252.

38. Watson, K.E., F. Parhami, V. Shin, and L.L. Demer, Fibronectin and collagen I matrixes promote calcification of vascular cells in vitro, whereas collagen IV matrix is inhibitory. Arterioscler Thromb Vasc Biol, 1998. **18**(12): p. 1964-71.

39. Rochette, L., A. Meloux, E. Rigal, M. Zeller, G. Malka, Y. Cottin, and C. Vergely, The Role of Osteoprotegerin in Vascular Calcification and Bone Metabolism: The Basis for Developing New Therapeutics. Calcif Tissue Int, 2019. **105**(3): p. 239-251.

40. Ciceri, P., E. Volpi, I. Brenna, F. Elli, E. Borghi, D. Brancaccio, and M. Cozzolino, The combination of lanthanum chloride and the calcimimetic calindol delays the progression of vascular smooth muscle cells calcification. Biochem Biophys Res Commun, 2012. **418**(4): p. 770-3.

41. Voelkl, J., F. Lang, K.U. Eckardt, K. Amann, O.M. Kuro, A. Pasch, B. Pieske, and I. Alesutan, Signaling pathways involved in vascular smooth muscle cell calcification during hyperphosphatemia. Cell Mol Life Sci, 2019. **76**(11): p. 2077-2091.

42. Chavkin, N.W., J.J. Chia, M.H. Crouthamel, and C.M. Giachelli, Phosphate uptake-independent signaling functions of the type III sodium-dependent phosphate transporter, PiT-1, in vascular smooth muscle cells. Exp Cell Res,

2015. **333**(1): p. 39-48.

43. Luong, T.T.D., N. Schelski, B. Boehme, M. Makridakis, A. Vlahou, F. Lang, B. Pieske, I. Alesutan, and J. Voelkl, Fibulin-3 Attenuates Phosphate-Induced Vascular Smooth Muscle Cell Calcification by Inhibition of Oxidative Stress. Cell Physiol Biochem, 2018. **46**(4): p. 1305-1316.

44. Chen, N.X., K.D. O'Neill, X. Chen, K. Kiattisunthorn, V.H. Gattone, and S.M. Moe, Activation of arterial matrix metalloproteinases leads to vascular calcification in chronic kidney disease. Am J Nephrol, 2011. **34**(3): p. 211-9.

45. Ponnusamy, A., S. Sinha, G.D. Hyde, S.J. Borland, R.F. Taylor, E. Pond, H.J. Eyre, C.A. Inkson, A. Gilmore, N. Ashton, P.A. Kalra, and A.E. Canfield, FTI-277 inhibits smooth muscle cell calcification by up-regulating PI3K/Akt signaling and inhibiting apoptosis. PLoS One, 2018. **13**(4): p. e0196232.

46. Voelkl, J., R. Tuffaha, T.T.D. Luong, D. Zickler, J. Masyout, M. Feger, N. Verheyen, F. Blaschke, O.M. Kuro, A. Tomaschitz, S. Pilz, A. Pasch, K.U. Eckardt, J.E. Scherberich, F. Lang, B. Pieske, and I. Alesutan, Zinc Inhibits Phosphate-Induced Vascular Calcification through TNFAIP3-Mediated Suppression of NF-kappaB. J Am Soc Nephrol, 2018. **29**(6): p. 1636-1648.

47. Voelkl, J., T.T. Luong, R. Tuffaha, K. Musculus, T. Auer, X. Lian, C. Daniel, D. Zickler, B. Boehme, M. Sacherer, B. Metzler, D. Kuhl, M. Gollasch, K. Amann, D.N. Muller, B. Pieske, F. Lang, and I. Alesutan, SGK1 induces vascular smooth muscle cell calcification through NF-kappaB signaling. J Clin Invest, 2018. **128**(7): p. 3024-3040.

48. Montes de Oca, A., F. Guerrero, J.M. Martinez-Moreno, J.A. Madueno, C. Herencia, A. Peralta, Y. Almaden, I. Lopez, E. Aguilera-Tejero, K. Gundlach, J. Buchel, M.E. Peter, J. Passlick-Deetjen, M. Rodriguez, and J.R. Munoz-Castaneda, Magnesium inhibits Wnt/beta-catenin activity and reverses the osteogenic transformation of vascular smooth muscle cells. PLoS One, 2014. **9**(2): p. e89525.

49. Lee, H.L., K.M. Woo, H.M. Ryoo, and J.H. Baek, Tumor necrosis factor-

alpha increases alkaline phosphatase expression in vascular smooth muscle cells via MSX2 induction. Biochem Biophys Res Commun, 2010. **391**(1): p. 1087-92.

50. Herrmann, J., M. Babic, M. Tolle, M. van der Giet, and M. Schuchardt, Research Models for Studying Vascular Calcification. Int J Mol Sci, 2020. **21**(6).

51. Adeney, K.L., D.S. Siscovick, J.H. Ix, S.L. Seliger, M.G. Shlipak, N.S. Jenny, and B.R. Kestenbaum, Association of serum phosphate with vascular and valvular calcification in moderate CKD. J Am Soc Nephrol, 2009. **20**(2): p. 381-7.

52. Bundy, J.D., J. Chen, W. Yang, M. Budoff, A.S. Go, J.E. Grunwald, R.R. Kallem, W.S. Post, M.P. Reilly, A.C. Ricardo, S.E. Rosas, X. Zhang, J. He, and C.S. Investigators, Risk factors for progression of coronary artery calcification in patients with chronic kidney disease: The CRIC study. Atherosclerosis, 2018. **271**: p. 53-60.

53. Shang, D., Q. Xie, X. Ge, H. Yan, J. Tian, D. Kuang, C.M. Hao, and T. Zhu, Hyperphosphatemia as an independent risk factor for coronary artery calcification progression in peritoneal dialysis patients. BMC Nephrol, 2015. **16**: p. 107.

54. Kidney Disease: Improving Global Outcomes, C.K.D.M.B.D.U.W.G., KDIGO 2017 Clinical Practice Guideline Update for the Diagnosis, Evaluation, Prevention, and Treatment of Chronic Kidney Disease-Mineral and Bone Disorder (CKD-MBD). Kidney Int Suppl (2011), 2017. **7**(1): p. 1-59.

55. Elion, G.B., S.W. Callahan, G.H. Hitchings, and R.W. Rundles, The metabolism of 2-amino-6-[(1-methyl-4-nitro-5-imidazolyl)thio]purine (B.W. 57-323) in man. Cancer Chemother Rep, 1960. **8**: p. 47-52.

56. Schwartz, R., J. Stack, and W. Dameshek, Effect of 6-mercaptopurine on antibody production. Proc Soc Exp Biol Med, 1958. **99**(1): p. 164-7.

57. Liefeldt, L. and K. Budde, Risk factors for cardiovascular disease in renal transplant recipients and strategies to minimize risk. Transpl Int, 2010. **23**(12):

p. 1191-204.

58. Marechal, C., E. Coche, E. Goffin, A. Dragean, G. Schlieper, P. Nguyen, J. Floege, N. Kanaan, O. Devuyst, and M. Jadoul, Progression of coronary artery calcification and thoracic aorta calcification in kidney transplant recipients. Am J Kidney Dis, 2012. **59**(2): p. 258-69.

59. Prufer, J., M. Schuchardt, M. Tolle, N. Prufer, M. Hohne, W. Zidek, and M. van der Giet, Harmful effects of the azathioprine metabolite 6-mercaptopurine in vascular cells: induction of mineralization. PLoS One, 2014. **9**(7): p. e101709.

60. Schuchardt, M., J. Herrmann, C. Henkel, M. Babic, M. van der Giet, and M. Tolle, Long-Term Treatment of Azathioprine in Rats Induces Vessel Mineralization. Biomedicines, 2021. **9**(3).

61. Herrmann, J., M.R. Gummi, M. Xia, M. van der Giet, M. Tolle, and M. Schuchardt, Vascular Calcification in Rodent Models-Keeping Track with an Extented Method Assortment. Biology (Basel), 2021. **10**(6).

62. Mulvany, M.J. and W. Halpern, Contractile properties of small arterial resistance vessels in spontaneously hypertensive and normotensive rats. Circ Res, 1977. **41**(1): p. 19-26.

63. Bevan, J.A. and J.V. Osher, A direct method for recording tension changes in the wall of small blood vessels in vitro. Agents Actions, 1972. **2**(5): p. 257-60.

64. Mulvany, M.J. and N. Nyborg, An increased calcium sensitivity of mesenteric resistance vessels in young and adult spontaneously hypertensive rats. Br J Pharmacol, 1980. **71**(2): p. 585-96.

65. Mulvany, M., Procedures for investigation of small vessels using small vessel myograph. Department of Pharmacology, Aarhus University, Denmark. latest revision: August, 2004.

66. Guedel, A.E., Stages of anesthesia and a re-classification of the signs of anesthesia. Anesthesia & Analgesia, 1927. **6**(4): p. 157-162.

67. Spiers, A. and N. Padmanabhan, A guide to wire myography. Methods Mol

Med, 2005. **108**: p. 91-104.

68. Gequelim, G.C., D.A. da Luz Veronez, G. Lenci Marques, C.H. Tabushi, and R.D.R. Loures Bueno, Thoracic aorta thickness and histological changes with aging: an experimental rat model. J Geriatr Cardiol, 2019. **16**(7): p. 580-584.

69. Canas, D., E.A. Herrera, C. Garcia-Herrera, D. Celentano, and B.J. Krause, Fetal Growth Restriction Induces Heterogeneous Effects on Vascular Biomechanical and Functional Properties in Guinea Pigs (Cavia porcellus). Front Physiol, 2017. **8**: p. 144.

70. Ameer, O.Z., I.M. Salman, A.P. Avolio, J.K. Phillips, and M. Butlin, Opposing changes in thoracic and abdominal aortic biomechanical properties in rodent models of vascular calcification and hypertension. Am J Physiol Heart Circ Physiol, 2014. **307**(2): p. H143-51.

71. Lillie, M.A. and J.M. Gosline, Mechanical properties of elastin along the thoracic aorta in the pig. J Biomech, 2007. **40**(10): p. 2214-21.

72. Halloran, P.F., Immunosuppressive drugs for kidney transplantation. N Engl J Med, 2004. **351**(26): p. 2715-29.

73. Gearry, R.B. and M.L. Barclay, Azathioprine and 6-mercaptopurine pharmacogenetics and metabolite monitoring in inflammatory bowel disease. J Gastroenterol Hepatol, 2005. **20**(8): p. 1149-57.

74. Tolle, M., A. Reshetnik, M. Schuchardt, M. Hohne, and M. van der Giet, Arteriosclerosis and vascular calcification: causes, clinical assessment and therapy. Eur J Clin Invest, 2015. **45**(9): p. 976-85.

75. Henaut, L., J.M. Chillon, S. Kamel, and Z.A. Massy, Updates on the Mechanisms and the Care of Cardiovascular Calcification in Chronic Kidney Disease. Semin Nephrol, 2018. **38**(3): p. 233-250.

76. Ketteler, M., H. Rothe, T. Kruger, P.H. Biggar, and G. Schlieper, Mechanisms and treatment of extraosseous calcification in chronic kidney disease. Nat Rev Nephrol, 2011. **7**(9): p. 509-16.

77. Ogawa, T. and K. Nitta, Pathogenesis and Management of Vascular Calcification in Patients with End-Stage Renal Disease. Contrib Nephrol, 2018. **196**: p. 71-77.

78. Holmar, J., H. Noels, M. Bohm, S. Bhargava, J. Jankowski, and S. Orth-Alampour, Development, establishment and validation of in vitro and ex vivo assays of vascular calcification. Biochem Biophys Res Commun, 2020. **530**(2): p. 462-470.

79. Gayrard, N., K. Muyor, C. Notarnicola, F. Duranton, B. Jover, and A. Argiles, Optimisation of cell and ex vivo culture conditions to study vascular calcification. PLoS One, 2020. **15**(3): p. e0230201.

80. Cocciolone, A.J., J.Z. Hawes, M.C. Staiculescu, E.O. Johnson, M. Murshed, and J.E. Wagenseil, Elastin, arterial mechanics, and cardiovascular disease. Am J Physiol Heart Circ Physiol, 2018. **315**(2): p. H189-H205.

81. Dobrin, P.B. and T.R. Canfield, Elastase, collagenase, and the biaxial elastic properties of dog carotid artery. Am J Physiol, 1984. **247**(1 Pt 2): p. H124-31.

82. Fonck, E., G. Prod'hom, S. Roy, L. Augsburger, D.A. Rufenacht, and N. Stergiopulos, Effect of elastin degradation on carotid wall mechanics as assessed by a constituent-based biomechanical model. Am J Physiol Heart Circ Physiol, 2007. **292**(6): p. H2754-63.

83. Kim, J., M.C. Staiculescu, A.J. Cocciolone, H. Yanagisawa, R.P. Mecham, and J.E. Wagenseil, Crosslinked elastic fibers are necessary for low energy loss in the ascending aorta. J Biomech, 2017. **61**: p. 199-207.

84. Gosling, R.G. and M.M. Budge, Terminology for describing the elastic behavior of arteries. Hypertension, 2003. **41**(6): p. 1180-2.

85. Mahutga, R.R., C.T. Schoephoerster, and V.H. Barocas, The Ring-Pull Assay for Mechanical Properties of Fibrous Soft Tissues - An Analysis of the Uniaxial Approximation and a Correction for Nonlinear Thick-Walled Tissues. Exp Mech, 2021. **61**(1): p. 53-66.

86. Gabriela Espinosa, M., M. Catalin Staiculescu, J. Kim, E. Marin, and J.E. Wagenseil, Elastic Fibers and Large Artery Mechanics in Animal Models of Development and Disease. J Biomech Eng, 2018. **140**(2).

87. Tsamis, A., J.T. Krawiec, and D.A. Vorp, Elastin and collagen fibre microstructure of the human aorta in ageing and disease: a review. J R Soc Interface, 2013. **10**(83): p. 20121004.

88. Zohora, F.-T., N. Nosoudi, S.R. Karamched, and N. Vyavahare, The Role of Elastin Degradation in Vascular Calcification: Possibilities to Repair Elastin and Reverse Calcification, in Cardiovascular Calcification and Bone Mineralization. 2020, Springer. p. 441-480.

89. Urry, D.W., Neutral sites for calcium ion binding to elastin and collagen: a charge neutralization theory for calcification and its relationship to atherosclerosis. Proc Natl Acad Sci U S A, 1971. **68**(4): p. 810-4.

90. Hosaka, N., M. Mizobuchi, H. Ogata, C. Kumata, F. Kondo, F. Koiwa, E. Kinugasa, and T. Akizawa, Elastin degradation accelerates phosphate-induced mineralization of vascular smooth muscle cells. Calcif Tissue Int, 2009. **85**(6): p. 523-9.

91. Pereira, L., S.Y. Lee, B. Gayraud, K. Andrikopoulos, S.D. Shapiro, T. Bunton, N.J. Biery, H.C. Dietz, L.Y. Sakai, and F. Ramirez, Pathogenetic sequence for aneurysm revealed in mice underexpressing fibrillin-1. Proc Natl Acad Sci U S A, 1999. **96**(7): p. 3819-23.

92. Luo, G., P. Ducy, M.D. McKee, G.J. Pinero, E. Loyer, R.R. Behringer, and G. Karsenty, Spontaneous calcification of arteries and cartilage in mice lacking matrix GLA protein. Nature, 1997. **386**(6620): p. 78-81.

93. Simionescu, D., A. Simionescu, and R. Deac, Detection of remnant proteolytic activities in unimplanted glutaraldehyde-treated bovine pericardium and explanted cardiac bioprostheses. J Biomed Mater Res, 1993. **27**(6): p. 821-9.

94. Vyavahare, N., P.L. Jones, S. Tallapragada, and R.J. Levy, Inhibition of

matrix metalloproteinase activity attenuates tenascin-C production and calcification of implanted purified elastin in rats. Am J Pathol, 2000. **157**(3): p. 885-93.

95. Wang, M., S.H. Kim, R.E. Monticone, and E.G. Lakatta, Matrix metalloproteinases promote arterial remodeling in aging, hypertension, and atherosclerosis. Hypertension, 2015. **65**(4): p. 698-703.

96. Basalyga, D.M., D.T. Simionescu, W. Xiong, B.T. Baxter, B.C. Starcher, and N.R. Vyavahare, Elastin degradation and calcification in an abdominal aorta injury model: role of matrix metalloproteinases. Circulation, 2004. **110**(22): p. 3480-7.

97. Aikawa, E., M. Aikawa, P. Libby, J.L. Figueiredo, G. Rusanescu, Y. Iwamoto, D. Fukuda, R.H. Kohler, G.P. Shi, F.A. Jaffer, and R. Weissleder, Arterial and aortic valve calcification abolished by elastolytic cathepsin S deficiency in chronic renal disease. Circulation, 2009. **119**(13): p. 1785-94.

98. Andrault, P.M., P. Panwar, N.C.W. Mackenzie, and D. Bromme, Elastolytic activity of cysteine cathepsins K, S, and V promotes vascular calcification. Sci Rep, 2019. **9**(1): p. 9682.

99. Sorushanova, A., L.M. Delgado, Z. Wu, N. Shologu, A. Kshirsagar, R. Raghunath, A.M. Mullen, Y. Bayon, A. Pandit, M. Raghunath, and D.I. Zeugolis, The Collagen Suprafamily: From Biosynthesis to Advanced Biomaterial Development. Adv Mater, 2019. **31**(1): p. e1801651.

100. Payne, L.S. and P.H. Huang, The pathobiology of collagens in glioma. Mol Cancer Res, 2013. **11**(10): p. 1129-40.

101. Gupta, P.B., T.T. Onder, G. Jiang, K. Tao, C. Kuperwasser, R.A. Weinberg, and E.S. Lander, Identification of selective inhibitors of cancer stem cells by high-throughput screening. Cell, 2009. **138**(4): p. 645-659.

102. Ratzinger, S., S. Grassel, A. Dowejko, T.E. Reichert, and R.J. Bauer, Induction of type XVI collagen expression facilitates proliferation of oral cancer cells. Matrix Biol, 2011. **30**(2): p. 118-25.

103. Manon-Jensen, T., N.G. Kjeld, and M.A. Karsdal, Collagen-mediated hemostasis. J Thromb Haemost, 2016. **14**(3): p. 438-48.

104. Lau, W.L. and J.H. Ix, Clinical detection, risk factors, and cardiovascular consequences of medial arterial calcification: a pattern of vascular injury associated with aberrant mineral metabolism. Semin Nephrol, 2013. **33**(2): p. 93-105.

105. Ahmad, P.J., D. Trcka, S. Xue, C. Franco, M.Y. Speer, C.M. Giachelli, and M.P. Bendeck, Discoidin domain receptor-1 deficiency attenuates atherosclerotic calcification and smooth muscle cell-mediated mineralization. Am J Pathol, 2009. **175**(6): p. 2686-96.

106. Roszkowska, M., A. Strzelecka-Kiliszek, L. Bessueille, R. Buchet, D. Magne, and S. Pikula, Collagen promotes matrix vesicle-mediated mineralization by vascular smooth muscle cells. J Inorg Biochem, 2018. **186**: p. 1-9.

107. Henaut, L., C. Boudot, Z.A. Massy, I. Lopez-Fernandez, S. Dupont, A. Mary, T.B. Drueke, S. Kamel, M. Brazier, and R. Mentaverri, Calcimimetics increase CaSR expression and reduce mineralization in vascular smooth muscle cells: mechanisms of action. Cardiovasc Res, 2014. **101**(2): p. 256-65.

108. Nikolov, I.G., N. Joki, T. Nguyen-Khoa, I.C. Guerrera, J. Maizel, J. Benchitrit, L. Machado dos Reis, A. Edelman, B. Lacour, V. Jorgetti, T.B. Drueke, and Z.A. Massy, Lanthanum carbonate, like sevelamer-HCl, retards the progression of vascular calcification and atherosclerosis in uremic apolipoprotein E-deficient mice. Nephrol Dial Transplant, 2012. **27**(2): p. 505-13.

109. Tyson, K.L., J.L. Reynolds, R. McNair, Q. Zhang, P.L. Weissberg, and C.M. Shanahan, Osteo/chondrocytic transcription factors and their target genes exhibit distinct patterns of expression in human arterial calcification. Arterioscler Thromb Vasc Biol, 2003. **23**(3): p. 489-94.

110. Lin, M.E., T. Chen, E.M. Leaf, M.Y. Speer, and C.M. Giachelli, Runx2

Expression in Smooth Muscle Cells Is Required for Arterial Medial Calcification in Mice. Am J Pathol, 2015. **185**(7): p. 1958-69.

111. Zhao, G., A.L. Raines, M. Wieland, Z. Schwartz, and B.D. Boyan, Requirement for both micron- and submicron scale structure for synergistic responses of osteoblasts to substrate surface energy and topography. Biomaterials, 2007. **28**(18): p. 2821-9.

112. Aronovich, A., Y. Nur, E. Shezen, C. Rosen, Y. Zlotnikov Klionsky, I. Milman, L. Yarimi, D. Hagin, G. Rechavi, U. Martinowitz, T. Nagasawa, P.S. Frenette, D. Tchorsh-Yutsis, and Y. Reisner, A novel role for factor VIII and thrombin/PAR1 in regulating hematopoiesis and its interplay with the bone structure. Blood, 2013. **122**(15): p. 2562-71.

113. Henaut, L. and Z.A. Massy, New insights into the key role of interleukin 6 in vascular calcification of chronic kidney disease. Nephrol Dial Transplant, 2018. **33**(4): p. 543-548.

114. Yu, C., C. Zhang, Z. Kuang, and Q. Zheng, The Role of NLRP3 Inflammasome Activities in Bone Diseases and Vascular Calcification. Inflammation, 2021. **44**(2): p. 434-449.

115. Shen, J., M. Zhao, C. Zhang, and X. Sun, IL-1beta in atherosclerotic vascular calcification: From bench to bedside. Int J Biol Sci, 2021. **17**(15): p. 4353-4364.

116. Sun, M., Q. Chang, M. Xin, Q. Wang, H. Li, and J. Qian, Endogenous bone morphogenetic protein 2 plays a role in vascular smooth muscle cell calcification induced by interleukin 6 in vitro. Int J Immunopathol Pharmacol, 2017. **30**(3): p. 227-237.

117. Chen, T.C., C.K. Yen, Y.C. Lu, C.S. Shi, R.Z. Hsieh, S.F. Chang, and C.N. Chen, The antagonism of 6-shogaol in high-glucose-activated NLRP3 inflammasome and consequent calcification of human artery smooth muscle cells. Cell Biosci, 2020. **10**: p. 5.

118. Intengan, H.D. and E.L. Schiffrin, Vascular remodeling in hypertension:

roles of apoptosis, inflammation, and fibrosis. Hypertension, 2001. **38**(3 Pt 2): p. 581-7.

119. Maki-Petaja, K.M., F.C. Hall, A.D. Booth, S.M. Wallace, Yasmin, P.W. Bearcroft, S. Harish, A. Furlong, C.M. McEniery, J. Brown, and I.B. Wilkinson, Rheumatoid arthritis is associated with increased aortic pulse-wave velocity, which is reduced by anti-tumor necrosis factor-alpha therapy. Circulation, 2006. **114**(11): p. 1185-92.

Statutory Declaration

“I, Jinwen Zhou, by personally signing this document in lieu of an oath, hereby affirm that I prepared the submitted dissertation on the topic: “Ex vivo measurement of biomechanical properties during vascular calcification; Ex vivo Messung biomechanischer Eigenschaften bei Gefäßverkalkung”, independently and without the support of third parties, and that I used no other sources and aids than those stated.

All parts which are based on the publications or presentations of other authors, either in letter or in spirit, are specified as such in accordance with the citing guidelines. The sections on methodology (in particular regarding practical work, laboratory regulations, statistical processing) and results (in particular regarding figures, charts and tables) are exclusively my responsibility.

Furthermore, I declare that I have correctly marked all of the data, the analyses, and the conclusions generated from data obtained in collaboration with other persons, and that I have correctly marked my own contribution and the contributions of other persons (cf. declaration of contribution). I have correctly marked all texts or parts of texts that were generated in collaboration with other persons.

My contributions to any publications to this dissertation correspond to those stated in the below joint declaration made together with the supervisor. All publications created within the scope of the dissertation comply with the guidelines of the ICMJE (International Committee of Medical Journal Editors; www.icmje.org) on authorship. In addition, I declare that I shall comply with the regulations of Charité – Universitätsmedizin Berlin on ensuring good scientific practice.

I declare that I have not yet submitted this dissertation in identical or similar form to another Faculty.

The significance of this statutory declaration and the consequences of a false statutory declaration under criminal law (Sections 156, 161 of the German Criminal Code) are known to me.”

_____	_____
Date	Signature

Curriculum Vitae

My curriculum vitae does not appear in the electronic version of my paper for reasons of data protection.

Acknowledgments

At this moment, I would like to express my gratitude to those who have supported me during my study in Germany.

First of all, I thank Prof. Dr. Markus van der Giet, Priv.-Doz. Dr. med. Markus Tölle and Dr. Mirjam Schuchardt gave me the opportunity to study at Charité – Universitätsmedizin Berlin and work in their group on this interesting project.

Additionally, I thank Dr. Mirjam Schuchardt and Priv.-Doz. Dr. med. Markus Tölle for the experimental design, evaluation of this thesis, and other support. They have been generous and meticulous in helping me, not only in academic research but also in daily life.

I thank Manasa and Anna for their support in my experiments.

I thank Katharina Kuschfeldt and Brigitte Egbers for their lab work assistance.

Finally, a heartfelt thanks to my entire family, especially my wife, Nana Hu, who offered me constant support and encouragement during my entire study and life in Berlin.

Confirmation by a statistician

CHARITÉ

CharitéCentrum für Human- und Gesundheitswissenschaften

Charité | Campus Charité Mitte | 10117 Berlin

Name, Vorname: Zhou, Jinwen
Emailadresse: jinwen.zhou@charite.de
Matrikelnummer: 227045
PromotionsbetreuerIn: Frau Dr. Mirjam Tölle-Schuchardt
Promotionsinstitution / Klinik: Medizinische Klinik für Nephrologie CBF

Institut für Biometrie und klinische Epidemiologie (IBikE)
Direktor: Prof. Dr. Geraldine Rauch
Postanschrift:
Charitéplatz 1 | 10117 Berlin
Besucheranschrift:
Reinhardtstr. 58 | 10117 Berlin
Tel. +49 (0)30 450 562171
geraldine.rauch@charite.de
https://biometrie.charite.de/

Bescheinigung

Hiermit bescheinige ich, dass Herr Zhou innerhalb der Service Unit Biometrie des Instituts für Biometrie und klinische Epidemiologie (iBikE) bei mir eine statistische Beratung zu einem Promotionsvorhaben wahrgenommen hat. Folgende Beratungstermine wurden wahrgenommen:

- Termin 1: 01.03.22

Folgende wesentliche Ratschläge hinsichtlich einer sinnvollen Auswertung und Interpretation der Daten wurden während der Beratung erteilt:

- Anstelle von parametrischen Tests lieber nicht-parametrische Tests nutzen aufgrund der kleinen Fallzahlen (Kruskall Wallis anstelle von ANOVA, Wilcoxen Test anstelle von t-Test für verbundene Stichproben)
- Mixed-model wäre sinnvoll, aufgrund der Messwiederholungen, dann können die Gruppen über die Zeit verglichen werden (Zeiten als random effects wählen)

Diese Bescheinigung garantiert nicht die richtige Umsetzung der in der Beratung gemachten Vorschläge, die korrekte Durchführung der empfohlenen statistischen Verfahren und die richtige Darstellung und Interpretation der Ergebnisse. Die Verantwortung hierfür obliegt allein dem Promovierenden. Das Institut für Biometrie und klinische Epidemiologie übernimmt hierfür keine Haftung.

Datum: 16.03.2022

CHARITÉ UNIVERSITÄTSMEDIZIN BERLIN Institut für Biometrie und Klinische Epidemiologie Campus Charité Mitte Charitéplatz 1 | 10117 Berlin Reinhardtstr. 58

Name der Beraterin: Nilufar Akbari

Unterschrift Beraterin, Institutsstempel